Journal of Computational Physics 229 (2010) 5573–5596

Contents lists available at ScienceDirect

Journal of Computational Physics

journal homepage: www.elsevier.com/locate/jcp

New interpolation technique for the CIP method on curvilinear coordinates

Nobuyoshi Fujimatsu [a,*], Kojiro Suzuki [b,**]

[a] Department of Mechanical Science and Engineering, Aoyama Gakuin University, 5-10-1 Kobuchi, Sagamihara, Kanagawa 229-8558, Japan
[b] Department of Advanced Energy, Graduate School of Frontier Sciences, University of Tokyo, 5-1-5 Kashiwanoha, Kashiwa, Chiba 227-8561, Japan

ARTICLE INFO

Article history:
Received 24 August 2009
Received in revised form 23 March 2010
Accepted 25 March 2010
Available online 29 March 2010

Keywords:
Curvilinear coordinate
Numerical algorithm
Semi-Lagrangian schemes

ABSTRACT

We propose a new interpolation technique for the CIP method applied to curvilinear coordinates. The CIP method can hardly maintain third-order accuracy on curvilinear coordinates. The reason for the degeneracy in accuracies has not been discussed in detail. This paper reveals the problems of the CIP method on curvilinear coordinates and presents an improved CIP method to solve the advection equation accurately. The features of the presented method are: (1) the metric computation on the upwind stencil is defined in the same manner as in the advection phase of the CIP method; and (2) gradient values in the physical domain in the computation on the curvilinear coordinates are used. Various test problems show that the improved CIP method has approximate third-order accuracy.

1. Introduction

The role of computational fluid dynamics (CFD) has been becoming more and more important in various engineering fields. For example, in aerospace engineering, CFD techniques are indispensable to estimate aerodynamic characteristics and investigate the flow field around vehicles. Numerical simulations are computed on curvilinear coordinates because most aerospace vehicles have complicated geometries. The use of curvilinear coordinates is also necessary to capture the boundary layer around a vehicle. There are numerous techniques to solve the flow equations. The CIP method is one such method [1]. The characteristics of this method are to interpolate variables between the stencils using a cubic function. In this method, the interpolation function is decided from the physical quantities and the gradient values of the variables defined on the grid points. When we apply the CIP method to complicated mesh geometries, we take two methods to denote the interpolation function on the mesh system. One is the extension to curvilinear coordinates by coordinate transformation [2]. The other is to construct a mesh system adapted to the CIP method. A Soroban grid is a reasonable mesh system for the CIP method [3]. However, the CIP method frequently encounters deterioration of accuracy when the advection equations are solved on curvilinear coordinates. In spite of various applications, this problem has not been resolved [2–5]. In the present paper, we propose a CIP method to solve the advection equations on curvilinear coordinates with high accuracy. In Section 2, the problems of the CIP method on curvilinear coordinates are investigated and an improved CIP method is proposed for computation on curvilinear coordinates. Section 3 discusses the extension of a multi-dimensional method.

* Corresponding author. Tel.: +81 42 7596218; fax: +81 42 7596502.
** Corresponding author.
E-mail address: fujimatu@me.aoyama.ac.jp (N. Fujimatsu).

0021-9991/$ - see front matter © 2010 Elsevier Inc. All rights reserved.
doi:10.1016/j.jcp.2010.03.039

2. One-dimensional CIP method

2.1. Physical coordinates

The advection equation in conservative form can be written as

$$\frac{\partial f}{\partial t}+\frac{\partial (uf)}{\partial x}=0 \tag{1}$$

Eq. (1) is rewritten by differential rules thus:

$$\frac{\partial f}{\partial t}+u\frac{\partial f}{\partial x}=H \tag{2}$$

Here,

$$H\equiv -f\frac{\partial u}{\partial x}$$

The CIP method defines the spline function that follows the advection equation. The cubic polynomial function used in the CIP method is decided to satisfy the advection equations and the spatial differentiation of that equation. When the differentiation of Eq. (2) is taken, we can obtain the following equation:

$$\frac{\partial f_x}{\partial t}+u\frac{\partial f_x}{\partial x}=H_x-u_x\frac{\partial f}{\partial x} \tag{3}$$

In the CIP method, Eqs. (2) and (3) are split into two phases: the advection phase and the non-advection phase.

Advection phase

$$\frac{\partial f}{\partial t}+u\frac{\partial f}{\partial x}=0 \tag{4}$$

$$\frac{\partial f_x}{\partial t}+u\frac{\partial f_x}{\partial x}=0 \tag{5}$$

Non-advection phase

$$\frac{\partial f}{\partial t}=-f\frac{\partial u}{\partial x} \tag{6}$$

$$\frac{\partial f_x}{\partial t}=H_x-u_x\frac{\partial f}{\partial x} \tag{7}$$

The CIP method solves the advection equations so that the numerical profiles satisfy those equations and their gradient. The profiles between grids are expressed by third-order polynomial as follows:

$$\begin{aligned} &f(x)=a_j x^3+b_j x^2+f_{x,j}x+f_j\\ &f_x(x)=3a_j x^2+2b_j x+f_{x,j}\\ &x=-u\Delta t \end{aligned} \tag{8}$$

The coefficients of the interpolation function can be decided from the continuous condition of the physical quantities and the gradient of those values between grid cells.

$$\begin{aligned} &f(x_j)=f_j\\ &f(x_j+\Delta x_{j+jsign/2})=f_{j+jsign}\\ &f_x(x_j)=f_{x,j}\\ &f_x(x_j+\Delta x_{j+jsign/2})=f_{x,j+jsign}\\ &\Delta x_{j+jsign/2}=jsign\cdot(x_{j+jsign}-x_j)\\ &jsign=-1(u\geqslant 0),\quad jsign=1(u<0) \end{aligned} \tag{9}$$

The coefficients of the interpolation function are obtained from Eqs. (8) and (9) as follows:

$$\begin{aligned} a_j&=jsign\frac{2(f_j-f_{j+jsign})}{\Delta x^3_{j+jsign/2}}+\frac{f_{x,j+jsign}+f_{x,j}}{\Delta x^2_{j+jsign/2}}\\ b_j&=\frac{3(f_{j+jsign}-f_j)}{\Delta x^2_{j+jsign/2}}+jsign\frac{f_{x,j+jsign}+2f_{x,j}}{\Delta x_{j+jsign/2}} \end{aligned} \tag{10}$$

The profiles are moved along Eq. (8). This is called the CIP method. Eqs. (4) and (5) are solved using the CIP method. Then an arbitrary method such as the finite difference method or finite element method is applied to Eqs. (6) and (7). We call this method based on Eq. (8) the original CIP method in the present paper [1].

2.2. Extension of the CIP method to the curvilinear coordinates

In one-dimensional problems, the CIP method is applied to a non-equally spaced grid. When we rewrite Eq. (1) to curvilinear coordinates using $\xi = \xi(x)$, the advection equations on the curvilinear coordinates can be obtained as follows:

$$\begin{aligned} &\frac{\partial f}{\partial t} + u\left(\xi_x \cdot \frac{\partial f}{\partial \xi}\right) = H' \\ &\frac{\partial f}{\partial t} + U\frac{\partial f}{\partial \xi} = H' \\ &H' \equiv -\left(\frac{u_\xi}{x_\xi}\right) f \end{aligned} \tag{11}$$

Here, $U = u/x_\xi$ and $\xi_x = 1/x_\xi$. The CIP function on the curvilinear coordinates is defined as in the previous section. When we take the differentiation of Eq. (11) with respect to ξ,

$$\frac{\partial f_\xi}{\partial t} + U\frac{\partial f_\xi}{\partial \xi} = H'_\xi - U_\xi \frac{\partial f}{\partial \xi}. \tag{12}$$

Eqs. (11) and (12) are split into two phases on the advection and the non-advection phases.

Advection phase

$$\frac{\partial f}{\partial t} + U\frac{\partial f}{\partial \xi} = 0 \tag{13}$$

$$\frac{\partial f_\xi}{\partial t} + U\frac{\partial f_\xi}{\partial \xi} = 0 \tag{14}$$

Non-advection phase

$$\frac{\partial f}{\partial t} = H' \tag{15}$$

$$\frac{\partial f_\xi}{\partial t} = H'_\xi - U_\xi \frac{\partial f}{\partial \xi} \tag{16}$$

Eqs. (13) and (14) are solved using the CIP method. Eqs. (15) and (16) in the non-advection phase can be solved by some kind of scheme. When we take the interpolation functions based on the CIP method in the previous section, we can obtain the coefficients of those functions as follows:

$$\begin{aligned} &F(\xi) = A_j\xi^3 + B_j\xi^2 + f_{\xi j}\xi + f_j \\ &F_\xi(\xi) = 3A_j\xi^2 + 2B_j\xi + f_{\xi j} \\ &\xi = -U\Delta t \end{aligned} \tag{17}$$

$$\begin{aligned} A_j &= jsign\frac{2(f_j - f_{j+jsign})}{\Delta\xi^3_{j+jsign/2}} + \frac{f_{\xi j+jsign} + f_{\xi j}}{\Delta\xi^2_{j+jsign/2}} \\ B_j &= \frac{3(f_{j+jsign} - f_j)}{\Delta\xi^2_{j+jsign/2}} + jsign\frac{f_{\xi j+jsign} + 2f_{\xi j}}{\Delta\xi_{j+jsign/2}} \\ jsign &= -1(U \geqslant 0), \quad jsign = 1(U < 0) \end{aligned} \tag{18}$$

In the present paper, the CIP method based on Eqs. (17) and (18) is called the CIP–CUV method [2,3]. To investigate the accuracy of the CIP–CUV method, we solve the scalar wave equation as a test problem [3]. For simplicity, the scalar velocity is constant in the computational domain. The initial profile is

$$\begin{aligned} &f(x, t=0) = 2 + sin(2\pi x) \\ &f_x(x, t=0) = 2\pi cos(2\pi x) \\ &\qquad 0(\leqslant x \leqslant 1) \end{aligned} \tag{19}$$

The numerical profiles after $t = 4.0$ are compared with the exact solution. The grid dependencies of the original CIP method and the CIP–CUV method are then investigated. The numerical error is evaluated using the following equation:

$$\epsilon = \frac{\sqrt{\sum_i^{MX}(f_{Num} - f_{exact})^2}}{\sum_i^{MX} f_{exact}} \tag{20}$$

where f_{Num} and f_{exact} are numerical and exact solutions, respectively, and MX corresponds to the number of grid points. The metrics can be calculated using the second order central difference scheme

$$x_{\xi j} = \frac{x_{j+1} - x_{j-1}}{2\Delta\xi} \tag{21}$$

The grid spacing changes at the center point discontinuously.

$$r(i) = \begin{cases} 1.0 & IL \leqslant i \leqslant IR \\ \alpha & \text{otherwise} \end{cases} \tag{22}$$

where $\alpha = (0.5, 1.0, 1.2, 1.5)$. Therefore, the mesh size is $\Delta x_i = \Delta x \cdot r(i)$ in which

$$\Delta x = 1 / \sum_{i=0}^{MX} r(i) \tag{23}$$

The number of grid points in the mesh is $MX = (100, 200, 500, 1000, 2000)$ for each α. $IL = MX/4$, $IR = IL + 20NM - 1$ and $NM = MX/100$ are applied to each of these numbers of grid points. The numerical results obtained by Eqs. (8) and (17) are shown in Figs. 1 and 2. Although the original CIP method maintains third-order accuracy independent of α, the numerical results obtained by the CIP–CUV method are less accurate than those of the original CIP method. Care must be taken in the application of the CIP–CUV method to the non-equally spaced grid.

2.3. Problems of the curvilinear coordinates CIP method and the improvement of the CIP method

In the present section, we investigate the deterioration of the accuracy of the CIP–CUV method. Although the treatment of the advection phase is quite different between Eqs. (8) and (17), the profiles of f and F must always coincide at each time step. It is of note to compare $F = F(\xi)$ at $\xi = -U_j \Delta t = -(\xi_{x,j} u)\Delta t$ and $f = f(x)$ at $x = -u\Delta t$. The profiles of F in the CIP–CUV method can be written by

$$\begin{aligned} F(\xi) &= A_j \xi^3 + B_j \xi^2 + f_{\xi,j}\xi + f_j = A_j(-U\Delta t)^3 + B_j(-U\Delta t)^2 + f_{\xi,j}(-U\Delta t) + f_j \\ &= A_j \xi_{x,j}^3 (-u\Delta t)^3 + B_j \xi_{x,j}^2 (-u\Delta t)^2 + f_{\xi,j}\xi_{x,j}(-u\Delta t) + f_j = A_j \xi_{x,j}^3 \cdot x^3 + B_j \xi_{x,j}^2 \cdot x^2 + f_{\xi,j}\xi_{x,j} \cdot x + f_j \end{aligned} \tag{24}$$

where $A_j \xi_{x,j}^3$ and $B_j \xi_{x,j}^3$ must correspond with a_j and b_j. Each coefficient can be rewritten as follows:

$$\begin{aligned} A_j \cdot \xi_{x,j}^3 &= \left[jsign \frac{2(f_j - f_{j+jsign})}{\Delta \xi_{j+jsign/2}^3} + \frac{f_{\xi,j+jsign} + f_{\xi,j}}{\Delta \xi_{j+jsign/2}^2} \right] \cdot \frac{1}{x_{\xi,j}^3} \\ &= \left[jsign \frac{2(f_j - f_{j+jsign})}{(\Delta \xi_{j+jsign/2} \cdot x_{\xi,j})^3} + \frac{(f_{\xi,j+jsign} + f_{\xi,j}) \cdot x_{\xi,j}}{(\Delta \xi_{j+jsign/2} \cdot x_{\xi,j})^2} \right] \neq a_j \end{aligned} \tag{25}$$

$$\begin{aligned} B_j \cdot \xi_{x,j}^2 &= \left[\frac{3(f_{j+jsign} - f_j)}{\Delta \xi_{j+jsign/2}^2} + jsign \frac{f_{\xi,j+jsign} + 2f_{\xi,j}}{\Delta \xi_{j+jsign/2}} \right] \cdot \frac{1}{x_{\xi,j}^2} \\ &= \left[\frac{3(f_{j+jsign} - f_j)}{(\Delta \xi_{j+jsign/2} \cdot x_{\xi,j})^2} + jsign \frac{(f_{\xi,j+jsign} + 2f_{\xi,j}) \cdot x_{\xi,j}}{(\Delta \xi_{j+jsign/2} \cdot x_{\xi,j})} \right] \neq b_j \end{aligned} \tag{26}$$

$$f_{\xi,j}\xi_{x,j} \neq f_{x,j} \tag{27}$$

The coefficients of Eqs. (25) and (26) would not generally coincide with those of Eq. (10). The denominator in Eq. (10) is expressed using the grid spacing in an upwind cell. However, $\Delta x_{j+jsign/2} \neq \Delta \xi_{j+jsign/2} \cdot x_{\xi,j}$ in general because metric x_ξ of Eqs. (25)

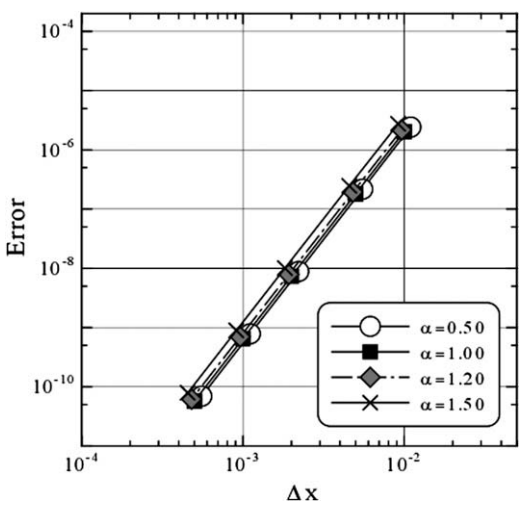

Fig. 1. Numerical results (Eq. (8)).

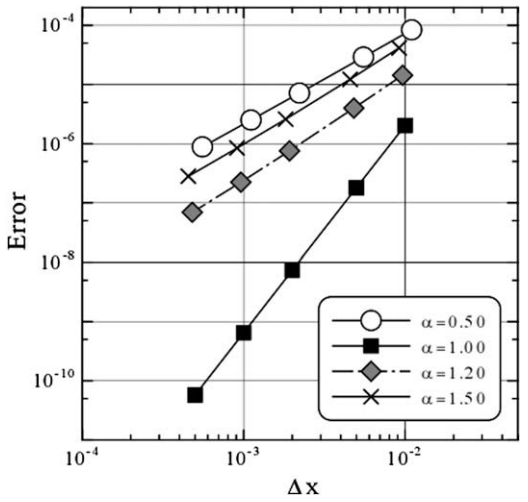

Fig. 2. Numerical results (Eq. (17)).

and (26) is evaluated by the central difference scheme. As long as the metrics are estimated by the central difference scheme, the coefficients of Eq. (18) do not agree with those of Eq. (10). In order to satisfy the equality condition, we should evaluate the metrics calculated using the same stencils as in the original CIP method. Although $f_\xi \xi_x = f_x$ is satisfied analytically, Eq. (27) is not consistent numerically. Therefore, the gradient of physical quantity f_ξ in the computational plane should be computed using the following expression $f_{\xi j} = f_{xj}/\xi_{xj}$. From the above discussion, the deterioration of accuracy of the CIP–CUV method is caused by inappropriate evaluation of the metrics and the gradient value of the physical quantities. Here, we rewrite the coefficients of interpolation function of the CIP–CUV method.

$$
\begin{aligned}
A_j \cdot \tilde{\xi}^3_{xj} &= \left[jsign \frac{2(f_j - f_{j+jsign})}{\Delta\xi^3_{j+jsign/2}} + \frac{\tilde{f}_{\xi j+jsign} + \tilde{f}_{\xi j}}{\Delta\xi^2_{j+jsign/2}} \right] \cdot \frac{1}{\tilde{x}^3_{\xi j+jsign/2}} \\
&= \left[jsign \frac{2(f_j - f_{j+jsign})}{(\Delta\xi_{j+jsign/2} \cdot \tilde{x}_{\xi j+jsign/2})^3} + \frac{(\tilde{f}_{\xi j+jsign} + \tilde{f}_{\xi j})/\tilde{x}_{\xi j+jsign/2}}{(\Delta\xi_{j+jsign/2} \cdot \tilde{x}_{\xi j+jsign/2})^2} \right] = a_j \\
B_j \cdot \tilde{\xi}^2_{xj} &= \left[\frac{3(f_{j+jsign} - f_j)}{\Delta\xi^2_{j+jsign/2}} + jsign \frac{\tilde{f}_{\xi j+jsign} + 2\tilde{f}_{\xi j}}{\Delta\xi_{j+jsign/2}} \right] \cdot \frac{1}{\tilde{x}^2_{\xi j+jsign/2}} \\
&= \left[\frac{3(f_{j+jsign} - f_j)}{(\Delta\xi_{j+jsign/2} \cdot \tilde{x}_{\xi j})^2} + jsign \frac{\tilde{f}_{\xi j+jsign} + 2\tilde{f}_{\xi j}}{(\Delta\xi_{j+jsign/2} \cdot \tilde{x}_{\xi j})} \right] \cdot \frac{1}{x^2_{\xi j+jsign/2}} = b_j \\
\tilde{f}_{\xi j+jsign} &= f_{xj+jsign} \cdot \tilde{x}_{\xi j+jsign/2} \\
\tilde{f}_{\xi j} &= f_{xj} \cdot \tilde{x}_{\xi j+jsign/2}
\end{aligned}
\tag{28}
$$

$\tilde{x}_{\xi j}$ is the metric computed by the same stencils used in the original CIP method. In order to satisfy consistency with the original CIP method, the metrics must be evaluated as $\tilde{x}_{\xi j} = \tilde{x}_{\xi j+jsign} = \tilde{x}_{\xi j+jsign/2}$ between the grid points of x_j and $x_{j+jsign}$. The gradient value of the profile can be written as follows:

$$
\begin{aligned}
F_\xi(\tilde{\xi}) &= 3A_j\tilde{\xi}^2 + 2B_j\tilde{\xi} + \tilde{f}_{\xi j} \\
&= 3A_j(-U\Delta t)^2 + 2B_j(-U\Delta t) + \tilde{f}_{\xi j} \\
&= 3A_j\tilde{\xi}^2_{xj}(-u\Delta t)^2 + 2B_j\tilde{\xi}_{xj}(-u\Delta t) + \tilde{f}_{\xi j} \\
&= \frac{1}{\tilde{\xi}_{xj}} \cdot (3a_j x^2 + 2b_j x + f_{xj}) = \frac{f_{xj}}{\tilde{\xi}_{xj}} = \tilde{f}_{\xi j}
\end{aligned}
\tag{29}
$$

We can obtain the gradient value in the physical plane by coordinate transformation thus:

$$
f_{xj} = \tilde{f}_{\xi j} \cdot \tilde{\xi}_{xj} \tag{30}
$$

The equation set of the reconstructed CIP method is summarized as follows:

$$
\begin{aligned}
F(\tilde{\xi}) &= A_j\tilde{\xi}^3 + B_j\tilde{\xi}^2 + \tilde{f}_{\xi j}\tilde{\xi} + f_j \\
F_\xi(\tilde{\xi}) &= 3A_j\tilde{\xi}^2 + 2B_j\tilde{\xi} + \tilde{f}_{\xi j}
\end{aligned}
\tag{31}
$$

$$A_j = \left[jsign \frac{2(f_j - f_{j+jsign})}{\Delta\xi^3_{j+jsign/2}} + \frac{\tilde{f}_{\xi j+jsign} + \tilde{f}_{\xi j}}{\Delta\xi^2_{j+jsign/2}} \right]$$

$$B_j = \left[\frac{3(f_{j+jsign} - f_j)}{\Delta\xi^2_{j+jsign/2}} + jsign \frac{\tilde{f}_{\xi j+jsign} + 2\tilde{f}_{\xi j}}{\Delta\xi_{j+jsign/2}} \right]$$

$$\tilde{f}_{\xi j+jsign} = f_{x j+jsign} \cdot \tilde{x}_{\xi j+jsign/2}$$

$$\tilde{f}_{\xi j} = f_{x j} \cdot \tilde{x}_{\xi j+jsign/2}$$

$$\tilde{\xi} = -U\Delta t = -\tilde{\xi}_{x j} \cdot u\Delta t \tag{32}$$

$$\tilde{x}_\xi = jsign \cdot (x_{j+jsign} - x_j)/\Delta\xi \tag{33}$$

The present method can obtain the same numerical results computed by the original CIP method because the numerical scheme based on Eqs. (31)–(33) exactly corresponds to the original CIP method.

2.4. General case of advection equation

The non-advection phase needs to be solved when the advection equation has a different velocity in space. In the original CIP method, the advection and non-advection equations are solved separately. At first, Eqs. (13) and (14) are solved using the original CIP method. The arbitrary numerical method can be applied to Eqs. (15) and (16) in the non-advection phase. In the present study, the non-advection equations are computed by the central difference scheme. The present method uses metric $\tilde{x}_\xi$ redefined to maintain the third-order accuracy of the original CIP method. The present CIP method needs two types of metric when the metric in the non-advection phase is estimated by the central difference scheme. Here, we consider the treatment of the non-advection equations. The present CIP method can obtain the exact gradient value f_x *without solving Eq. (5)* because the present CIP method is equivalent to the original CIP method. Therefore, we can also solve Eq. (7) after Eq. (14) is solved in the advection phase.

Eqs. (7) and (16) are compared to investigate the appropriate non-advection equations. Table 1 shows the governing equations used in each numerical scheme. In case 2, $\tilde{f}_\xi$ is transformed inversely before solving the non-advection equation and f_x is computed. Then, Eq. (7) is solved in the non-advection phase. Case 3 takes Eq. (16) for $\tilde{f}_\xi$ as the non-advection equation.

When the advection velocity is different in space and time, the advection velocity must be carefully evaluated. Yabe et al.[3] proposed that the advection velocity should be evaluated as $\bar{u}_j = (u_j + u_{jup})/2$ of u_j at x_j and u_{jup} at $x_{jup} = x_j - u_j\Delta t$ to maintain the numerical accuracy. The advection velocity is also evaluated using their method in the present problem.

Here, wave propagation with different velocity in space is solved on curvilinear coordinates[3]. The computational domain has unit length. The profile of $f(x) = \exp(-(x-0.2)^2/0.05^2)$ and $f_x(x) = -2(x-0.2)/0.05^2 \cdot \exp[-(x-0.2)^2/0.05^2]$ is imposed as the initial condition. The velocity profile in the computational domain is $u = 1/(1+ax)$. The grid spacing is decided using Eq. (34).

$$r(i) = \begin{cases} 1.0 + \beta sin(2\pi(i - IL)/(IR - IL)) & IL \leqslant i \leqslant IR \\ 1.0 & \text{otherwise} \end{cases} \tag{34}$$

where $\beta = (0.0, 0.1, 0.2, 0.3, 0.5)$. The grid spacing at each location is defined as $\Delta x_i = \Delta x \cdot r(i)$. Δx is computed by Eq. (23). The time step is fixed at $\Delta t = 0.2 \cdot \Delta x$. The total number of grid points varies with $MX = (100, 200, 500, 1000, 2000)$. $IL = MX/4$, $IR = IL + 60NM - 1$ and $NM = MX/100$ are applied to each of these numbers of grid points. Boundary condition is derived analytically and imposed at the stencils. Numerical results after $t = 0.4$ are compared with the analytic solution. Numerical error is calculated using Eq. (20). Metrics x_ξ in the non-advection phase are evaluated by Eq. (21). Although the velocity gradient u_x can be computed analytically, we evaluate u_x as $\xi_x u_\xi$ in the present test. Note that the non-advection terms are solved by the fourth order Runge–Kutta method to maintain the numerical accuracy of the CIP method.

Fig. 3 shows the numerical results obtained by case 1D-1. The accuracy of the CIP–CUV method is less than second order accuracy even when the grid spacing is slightly changed ($\beta = 0.1$). These results mean that the original CIP method should not be applied to curvilinear coordinates. Fig. 4 shows the results of case 1D-2. Third-order accuracy can be maintained in all cases when Eq. (3) is solved as the non-advection equation. Fig. 5 shows the results of case 1D-3. There is no difference between the results of case 1D-1 and 1D-3. Case 1D-3 can not maintain high order accuracy and Eq. (16) is not appropriate as the non-advection equation. U_ξ contains information greater than two stencils because U in Eq. (16) has the metric evaluated

Table 1
One-dimensional cases.

Case	CIP method	Advection eqs.	Value	Metric	Non-advection eqs.	Value	Metric
1D-1	CIP–CUV	Eqs. (13) and (14)	f, f_ξ	Eq. (21)	Eqs. (15) and (16)	f, f_ξ	Eq. (21)
1D-2	Present 1	Eqs. (13) and (14)	$f, \tilde{f}_\xi$	Eq. (33)	Eqs. (6) and (7)	f, f_x	Eq. (21)
1D-3	Present 2	Eqs. (13) and (14)	$f, \tilde{f}_\xi$	Eq. (33)	Eqs. (15) and (16)	$f, \tilde{f}_\xi$	Eq. (21)

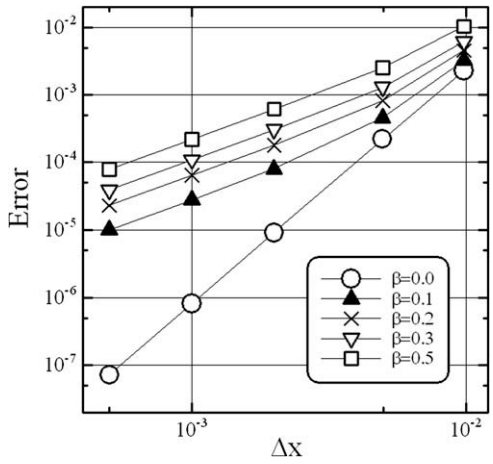

Fig. 3. CIP–CUV method (case 1D-1).

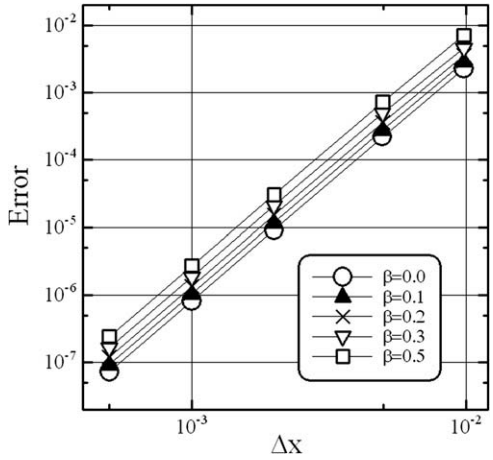

Fig. 4. Present CIP method (case 1D-2).

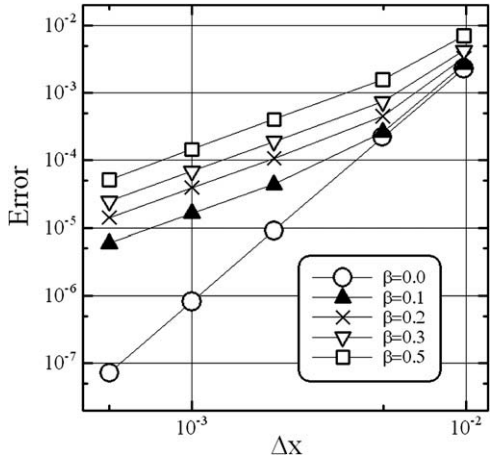

Fig. 5. Present CIP method (case 1D-3).

by the central difference scheme. The computation of u_x in Eq. (7) is sufficient in only two stencils. Therefore, the use of Eq. (16) does not fit the non-advection phase. From these results, the CIP method on curvilinear coordinates should solve the equation sets on physical coordinates.

The present method may require larger computational memory to use two different metrics for the advection and non-advection phases and imposes computational time for the coordinate transformation of the gradient variables. Table 2 shows the comparison of the computational time and the metrics used in the CIP–CUV method and present CIP method. These results are obtained at $MX = 2000$ in the test problem in Section 2.4. In case 1D-2(1), the increment of computational time corresponds to 3% although metrics $\tilde{x}_\xi$ and x_ξ in each phase are memorized in the computer. Even when metrics $\tilde{x}_\xi$ in the advection phase are computed at each time step, the computational time of the present method is larger than that of the CIP–CUV method only by 12%.

2.5. Investigation on the present method

One of the features in the CIP scheme is to advect the gradient value based on the governing equation. The present method uses f_ξ in the advection phase and f_x in the non-advection phase when the gradient value is solved. Can the gradient values on different coordinates be used to solve the advection and non-advection equations in each phase? Here, we investigate this numerical procedure based on the gradient advection equations.

The advection and the non-advection equations of the gradient value f_ξ can be written as

$$\frac{\partial f_\xi}{\partial t} + U\frac{\partial f_\xi}{\partial \xi} = 0 \tag{35}$$

$$\frac{\partial f_\xi}{\partial t} = -U_\xi f_\xi - \frac{\partial}{\partial \xi}\left(\frac{u_\xi}{x_\xi} f\right) \tag{36}$$

Eq. (35) is solved using the present CIP method and f_ξ is converted to f_x after advection. This numerical procedure means that Eq. (35) is transformed to physical coordinates.

$$\frac{1}{x_\xi}\left(\frac{\partial f_\xi}{\partial t} + U\frac{\partial f_\xi}{\partial \xi}\right) = 0 \tag{37}$$

$$\frac{\partial f_x}{\partial t} + \xi_x u\frac{\partial}{\partial x}\left(\frac{1}{\xi_x} f_x\right) = 0 \tag{38}$$

$$\frac{\partial f_x}{\partial t} + u\frac{\partial f_x}{\partial x} = -\left[\xi_x u\frac{\partial}{\partial x}\left(\frac{1}{\xi_x} f_x\right)\right] = Residual \tag{39}$$

Eq. (39) contains the residual term caused by the coordinate transformation. However, the residual term does not need to be solved as discussed below. In the CIP method, the right-hand side (RHS) of Eq. (39) is treated as the non-advection term. When f_ξ in Eq. (36) is also converted to f_x by coordinate transformation, we obtain Eq. (41).

$$\frac{1}{x_\xi}\frac{\partial f_x}{\partial t} = \frac{1}{\xi_x}\left[-U_\xi f_\xi - \frac{\partial}{\partial \xi}\left(\frac{u_\xi}{x_\xi} f\right)\right] \tag{40}$$

$$\frac{\partial f_x}{\partial t} = -\frac{\partial}{\partial \xi}(\xi_x u) f_x - \frac{\partial}{\partial x}(u_x f) \tag{41}$$

In the non-advection phase, the residual term in Eq. (39) is added to the RHS of Eq. (41).

$$\frac{\partial f_x}{\partial t} = -\frac{\partial}{\partial \xi}(\xi_x u) f_x - \frac{\partial}{\partial x}(u_x f) + Residual \tag{42}$$

The rearranged form of Eq. (42) can be written as

$$\frac{\partial f_x}{\partial t} = -\frac{\partial}{\partial \xi}(\xi_x u) f_x - \frac{\partial}{\partial x}(u_x f) - \left[\xi_x u\frac{\partial}{\partial x}\left(\frac{1}{\xi_x} f_x\right)\right] = -\frac{\partial}{\partial x}(u_x f) - u_x\frac{\partial f}{\partial x} = H_x - u_x\frac{\partial f}{\partial x} \tag{43}$$

The residual term in Eq. (39) is canceled by the terms on the RHS of Eq. (36) and we obtain Eq. (3). This investigation means that the gradient advection equations on curvilinear coordinates can be transformed to physical coordinates and vice versa. Therefore, the non-advection equation on the physical coordinates can be solved after the computation of the advection equation on the curvilinear coordinates.

Table 2
Comparison of the CIP–CUV and the present CIP method in the one-dimensional case.

Case	CIP method	CPU time (s)	Time ratio to the CIP–CUV	Metric in advection
1D-1	CIP–CUV	6.31	1.00	Memorized
1D-2(1)	Present 1	6.52	1.03	Memorized
1D-2(2)	Present 1	7.05	1.12	Not memorized

3. Two-dimensional CIP method in curvilinear coordinates

In this section, we extend the present CIP method to a two-dimensional method. The advection equation in two dimensions can be written as follows:

$$\frac{\partial f}{\partial t}+\frac{\partial (uf)}{\partial x}+\frac{\partial (vf)}{\partial y}=0 \tag{44}$$

$$\frac{\partial f}{\partial t}+u\frac{\partial f}{\partial x}+v\frac{\partial f}{\partial y}=-f\left(\frac{\partial u}{\partial x}+\frac{\partial v}{\partial y}\right) \tag{45}$$

When Eq. (45) is rewritten on the curvilinear coordinates,

$$\frac{\partial f}{\partial t}+U\frac{\partial f}{\partial \xi}+V\frac{\partial f}{\partial \eta}=H \tag{46}$$

$$H=-f\left(\xi_x\frac{\partial u}{\partial \xi}+\eta_x\frac{\partial u}{\partial \eta}+\xi_y\frac{\partial v}{\partial \xi}+\eta_y\frac{\partial v}{\partial \eta}\right)$$

where $U=\xi_x u+\xi_y v,\ V=\eta_x u+\eta_y v$.

The gradient advection equation can be derived in the same manner as in the one-dimensional case. We take the differentiations of Eq. (46) for ξ and η.

$$\frac{\partial f_\xi}{\partial t}+U\frac{\partial f_\xi}{\partial \xi}+V\frac{\partial f_\xi}{\partial \eta}=H_\xi-\left(U_\xi\frac{\partial f}{\partial \xi}+V_\xi\frac{\partial f}{\partial \eta}\right) \tag{47}$$

$$\frac{\partial f_\eta}{\partial t}+U\frac{\partial f_\eta}{\partial \xi}+V\frac{\partial f_\eta}{\partial \eta}=H_\eta-\left(U_\eta\frac{\partial f}{\partial \xi}+V_\eta\frac{\partial f}{\partial \eta}\right) \tag{48}$$

Eqs. (46)–(48) are split into the advection and the non-advection equations.

Advection phase

$$\frac{\partial f}{\partial t}+U\frac{\partial f}{\partial \xi}+V\frac{\partial f}{\partial \eta}=0 \tag{49}$$

$$\frac{\partial f_\xi}{\partial t}+U\frac{\partial f_\xi}{\partial \xi}+V\frac{\partial f_\xi}{\partial \eta}=0 \tag{50}$$

$$\frac{\partial f_\eta}{\partial t}+U\frac{\partial f_\eta}{\partial \xi}+V\frac{\partial f_\eta}{\partial \eta}=0 \tag{51}$$

Non-advection phase

$$\frac{\partial f}{\partial t}=H \tag{52}$$

$$\frac{\partial f_\xi}{\partial t}=H_\xi-\left(U_\xi\frac{\partial f}{\partial \xi}+V_\xi\frac{\partial f}{\partial \eta}\right) \tag{53}$$

$$\frac{\partial f_\eta}{\partial t}=H_\eta-\left(U_\eta\frac{\partial f}{\partial \xi}+V_\eta\frac{\partial f}{\partial \eta}\right) \tag{54}$$

There are two kinds of multi-dimensional methods for the CIP method. One is the directional splitting method to separately solve the advection equation for each direction. The other is to construct the interpolation function in the multi-dimension. At first, we extend the present CIP method to a multi-dimensional solution based on a splitting technique.

3.1. Extension to multi-dimensional scheme by the splitting technique

When we apply the directional splitting method, the advection equations (Eqs. (49)–(51)) are split into two equations with respect to each direction. First, the numerical profiles of f, f_ξ and f_η are advanced to ξ direction.

$$\frac{\partial f}{\partial t}+U\frac{\partial f}{\partial \xi}=0 \tag{55}$$

$$\frac{\partial f_\xi}{\partial t}+U\frac{\partial f_\xi}{\partial \xi}=0 \tag{56}$$

$$\frac{\partial f_\eta}{\partial t}+U\frac{\partial f_\eta}{\partial \xi}=0 \tag{57}$$

Second, the physical quantities of f, f_ξ and f_η are solved to η direction.

$$\frac{\partial f}{\partial t} + V\frac{\partial f}{\partial \eta} = 0 \tag{58}$$

$$\frac{\partial f_\xi}{\partial t} + V\frac{\partial f_\xi}{\partial \eta} = 0 \tag{59}$$

$$\frac{\partial f_\eta}{\partial t} + V\frac{\partial f_\eta}{\partial \eta} = 0 \tag{60}$$

An M-type CIP scheme[6] is used as the splitting technique. This method takes the following procedures.

1. Eqs. (61) and (62) are solved by the CIP method to advance the profile in ξ direction. Eq. (63) is solved by the 1st order upwind scheme. The numerical profiles are advanced using the following equations:

$$F(\xi) = A\xi^3 + B\xi^2 + f_\xi\xi + f \tag{61}$$

$$F_\xi(\xi) = 3A\xi^2 + 2B\xi + f_\xi \tag{62}$$

$$F_\eta(\xi) = f_\eta - U\Delta t\frac{f_{\eta j+jsign,k} - f_{\eta j,k}}{jsign\Delta\xi} \tag{63}$$

$$U = \xi_x u + \xi_y v$$

$$jsign = -1(U \geqslant 0), \quad jsign = 1(U < 0)$$

2. Eqs. (64) and (65) are solved by the CIP method to advance the profile in η direction. Eq. (66) is solved by the first-order upwind scheme. The numerical scheme can be written in the same manner as for ξ direction.

$$F(\eta) = A\eta^3 + B\eta^2 + f_\eta\eta + f \tag{64}$$

$$F_\eta(\eta) = 3A\eta^2 + 2B\eta + f_\eta \tag{65}$$

$$F_\xi(\eta) = f_\xi - V\Delta t\frac{f_{\xi j,k+ksign} - f_{\xi j,k}}{ksign\Delta\eta} \tag{66}$$

$$V = \eta_x u + \eta_y v$$

$$ksign = -1(V \geqslant 0), \quad ksign = 1(V < 0)$$

The M-type CIP scheme is based on the empirical fact that (1) an advection equation is needed to accurately solve for the direction of the advection, and (2) a numerical scheme with high accuracy is not required to solve the advection equation for the direction perpendicular to that of the advection.

In the CIP–CUV method, the coefficient of the CIP function and the contravariant velocity are computed from Eqs. (17) and (18). The numerical variables in the CIP–CUV method are f, f_ξ and f_η. Coordinate transformation is not needed to obtain the gradient valiables on the curvilinear coordinates. The metrics in the CIP–CUV method are computed by the second order central difference scheme and are unique in the advection and the non-advection phases. J is the jacobian.

$$\begin{aligned}
x_{\xi_{j,k}} &= \left(\frac{\eta_y}{J}\right)_{j,k} = (x_{j+1,k} - x_{j-1,k})/2\Delta\xi \\
x_{\eta_{j,k}} &= \left(-\frac{\xi_y}{J}\right)_{j,k} = (x_{j,k+1} - x_{j,k-1})/2\Delta\eta \\
y_{\xi_{j,k}} &= \left(-\frac{\eta_x}{J}\right)_{j,k} = (y_{j+1,k} - y_{j-1,k})/2\Delta\xi \\
y_{\eta_{j,k}} &= \left(\frac{\xi_x}{J}\right)_{j,k} = (y_{j,k+1} - y_{j,k-1})/2\Delta\eta \\
J_{j,k} &= \frac{1}{x_{\xi_{j,k}}y_{\eta_{j,k}} - x_{\eta_{j,k}}y_{\xi_{j,k}}}
\end{aligned} \tag{67}$$

The present CIP method uses Eqs. (32) and (33) to compute the coefficients and the velocities. The coefficients of the interpolation function A and B contain the gradient variables. When the present CIP scheme is applied to the advection phase, the gradient values $\tilde{f}_\xi, \tilde{f}_\eta$ are computed by coordinate transformation (Eq. (68)).

$$\begin{pmatrix} \tilde{f}_\xi \\ \tilde{f}_\eta \end{pmatrix} = \begin{pmatrix} \tilde{x}_\xi & \tilde{y}_\xi \\ \tilde{x}_\eta & \tilde{y}_\eta \end{pmatrix} \begin{pmatrix} f_x \\ f_y \end{pmatrix} \tag{68}$$

In the present CIP scheme, different metrics are used in the advection and the non-advection phases. The metrics in the advection phase are evaluated using the stencils of the CIP interpolation and are computed by the following equations.

$$\tilde{x}_{\xi j,k} = jsign(x_{j+jsign,k} - x_{j,k})/\Delta\xi = \left(\frac{\tilde{\eta}_y}{\tilde{J}}\right)_{j,k}$$
$$\tilde{x}_{\eta j,k} = ksign(x_{j,k+ksign} - x_{j,k})/\Delta\xi = -\left(\frac{\tilde{\xi}_y}{\tilde{J}}\right)_{j,k}$$
$$\tilde{y}_{\xi j,k} = jsign(y_{j+jsign,k} - x_{j,k})/\Delta\eta = -\left(\frac{\tilde{\eta}_x}{\tilde{J}}\right)_{j,k}$$
$$\tilde{y}_{\eta j,k} = ksign(y_{j,k+ksign} - x_{j,k})/\Delta\eta = \left(\frac{\tilde{\xi}_x}{\tilde{J}}\right)_{j,k}$$
$$\tilde{J}_{j,k} = \frac{1}{\tilde{x}_{\xi j,k}\tilde{y}_{\eta j,k} - \tilde{y}_{\xi j,k}\tilde{x}_{\eta j,k}} \tag{69}$$

One of the features in the present CIP scheme is to use the gradient value of the different coordinates in each phase. Before computing the non-advection phase, the gradient values advanced by the present CIP scheme are inversely transformed to the values in the physical domain using Eq. (70).

$$\begin{pmatrix} f_x \\ f_y \end{pmatrix} = \begin{pmatrix} \tilde{\xi}_x & \tilde{\eta}_x \\ \tilde{\xi}_y & \tilde{\eta}_y \end{pmatrix} \begin{pmatrix} \tilde{f}_\xi \\ \tilde{f}_\eta \end{pmatrix} \tag{70}$$

$\tilde{\xi}_x$, $\tilde{\xi}_y$, $\tilde{\eta}_x$ and $\tilde{\eta}_y$ are computed from Eq. (69). Eqs. (50), (51), (53) and (54) can be also rewritten on the physical coordinates when f_x and f_y are computed by inverse transformation in the non-advection phase. Non-advection equations are solved by the central difference scheme.

Fig. 6 shows the concept of coordinate transformation between the physical and computational planes. The physical plane is projected onto the computational plane with an orthogonal grid. The stencils of $\vec{r}_{j,k}$, $\vec{r}_{j+jsign,k}$, $\vec{r}_{j+jsign,k+ksign}$ and $\vec{r}_{j,k+ksign}$ in an upwind cell correspond to those of $\vec{\Gamma}_{j,k}$, $\vec{\Gamma}_{j+jsign,k}$, $\vec{\Gamma}_{j+jsign,k+ksign}$ and $\vec{\Gamma}_{j,k+ksign}$, respectively. P corresponds to the locations in the upwind cell on the physical plane and P' is that on the computational plane. The physical quantities at location P' are advected by the CIP method.

$$\begin{aligned} \xi &= \alpha xy + \beta x + \gamma y \\ \eta &= \alpha' xy + \beta' x + \gamma' y \\ x &= -u\Delta t \\ y &= -v\Delta t \end{aligned} \tag{71}$$

The accuracy of the CIP method depends on the locations of ξ and η in the upwind cell[3]. In order to denote the coordinate, there are some kinds of smooth function, e.g. polynomial interpolation, rational function interpolation, or cubic spline interpolation. We can apply these functions as the coordinate function to the present method. However, these functions usually consume much of computational time. In the present paper, we define the semi-nonlinear coordinate function as Eq. (71) to compute those locations accurately and to save the computational cost. The coordinates on the computational plane are defined using the four stencils on the physical coordinates. Location P' can be decided using Eq. (71) from location P when the form of the coordinate function is decided. The coefficients of α, β and γ in Eq. (71) are decided from the physical coordinates of an upwind. Locations ξ and η in the upwind cell and the metrics at each node can be computed using Eq. (71). The

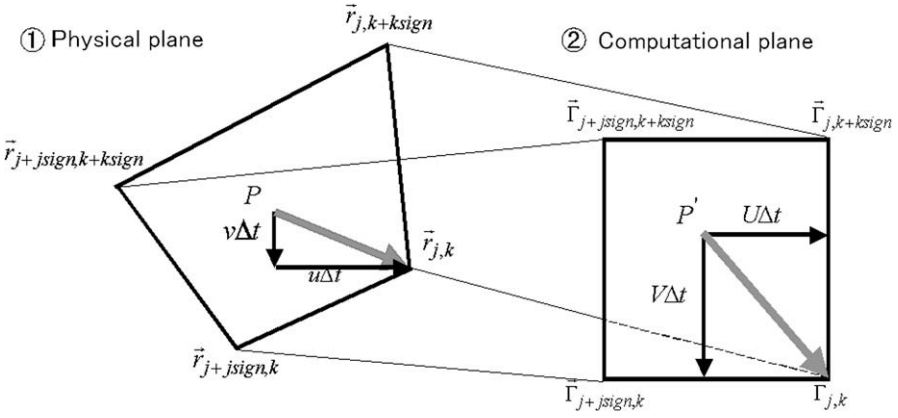

Fig. 6. Concept of the coordinate transform.

computation of the coefficient in Eq. (71) requires the inverse of the matrix. When the coordinates with the index of $(j+jsign, k+ksign)$ are not used for coordinate transformation, the coordinate function is a linear function ($\alpha = 0$ and $\alpha' = 0$). However, the maximum CFL number is restricted by 0.5 in general when the stencil at $(j+jsign, k+ksign)$ is not used. In the orthogonal grid, $\alpha = 0,\ \gamma = 0,\ \alpha' = 0$ and $\beta' = 0$, automatically. In the linear coordinate function, $\beta,\ \gamma,\ \beta'$ and γ' correspond to metrics $\tilde{\xi}_x,\ \tilde{\xi}_y,\ \tilde{\eta}_x$ and $\tilde{\eta}_y$, respectively, in Eq. (70).

3.1.1. Non-advection equations for the present CIP scheme

In the present CIP method, the non-advection equations on the physical coordinates are projected and solved to the curvilinear coordinates.

$$\frac{\partial f}{\partial t} = H \tag{72}$$

Take the differentiation of Eq. (72) to derivate the non-advection equations on the gradient value for the physical coordinates.

$$\frac{\partial f_x}{\partial t} = H_x - \frac{\partial u}{\partial x} f_x + \frac{\partial v}{\partial x} f_y \tag{73}$$

$$\frac{\partial f_y}{\partial t} = H_y - \frac{\partial u}{\partial y} f_x + \frac{\partial v}{\partial y} f_y \tag{74}$$

The spatial derivatives in the equations are transformed to curvilinear coordinates using the chain rule when solving the non-advection phase.

$$\begin{aligned} \frac{\partial H}{\partial x} &= \xi_x \frac{\partial H}{\partial \xi} + \eta_x \frac{\partial H}{\partial \eta} \\ \frac{\partial H}{\partial y} &= \xi_y \frac{\partial H}{\partial \xi} + \eta_y \frac{\partial H}{\partial \eta} \end{aligned} \tag{75}$$

$u_x,\ u_y,\ v_x$ and v_y are also computed using the differential chain rule as for Eq. (75) (H is replaced by u or v). The metrics in the non-advection phase are evaluated by the second order central difference scheme in the same manner as the one-dimensional case.

Table 3 shows the governing equations used in the CIP–CUV method, the present CIP method and the present CIP method with semi-nonlinear function. The non-advection equations in Table 2 are solved after the advection equations are computed by the CIP–CUV method or the present CIP method.

3.2. Solid revolution problem over the wavy grid

The solid revolution problem is solved as the test problem in the multi-dimensional case to investigate the ability of the present CIP method. A wavy grid is created using Eq. (76)[7].

$$\begin{aligned} x_0 &= (j-1)/(MX-1) \\ y_0 &= (k-1)/(MY-1) \\ x_{j,k} &= 100 \cdot (x_0 + 0.03 sin(2\pi\alpha y_0)) \\ y_{j,k} &= 100 \cdot (y_0 + 0.03 sin(2\pi\alpha x_0)) \end{aligned} \tag{76}$$

where $\alpha = (0, 1, 2, 3)$. $\alpha = 0$ corresponds to the orthogonal grid. The number of grid points of the mesh is changed with $MX = (50, 100, 200, 500, 1000)$. In all computations, MX is equivalent to MY. Fig. 7 shows the computational grids with $\alpha = (1, 2, 3)$.

The center of rotation is located at $(x_c, y_c) = (50, 50)$. The initial profile is

$$f(x,y) = \begin{cases} \frac{1+cos\left(\pi\sqrt{(x-x_c)^2+(y-y_c)^2}/R\right)}{2} & (x-x_c)^2 + (y-y_c)^2 < R \\ 0 & \text{otherwise} \end{cases} \tag{77}$$

Table 3
Two-dimensional test cases.

Case	CIP	Advection eqs.	Value	Metric	Non-advection eqs.	Value	Metric	Coordinate function
2D-1	CIP–CUV	Eqs. (49)–(51)	f, f_ξ, f_η	Eq. (67)	Eqs. (52)–(54)	f, f_ξ, f_η	Eq. (67)	Not used
2D-2	Present	Eqs. (49)–(51)	$f, \tilde{f}_\xi, \tilde{f}_\eta$	Eq. (69)	Eqs. (72)–(74)	f, f_x, f_y	Eq. (67)	Linear ($\alpha = 0$)
2D-3	Present	Eqs. (49)–(51)	$f, \tilde{f}_\xi, \tilde{f}_\eta$	Eq. (71)	Eqs. (72)–(74)	f, f_x, f_y	Eq. (67)	Semi-nonlinear

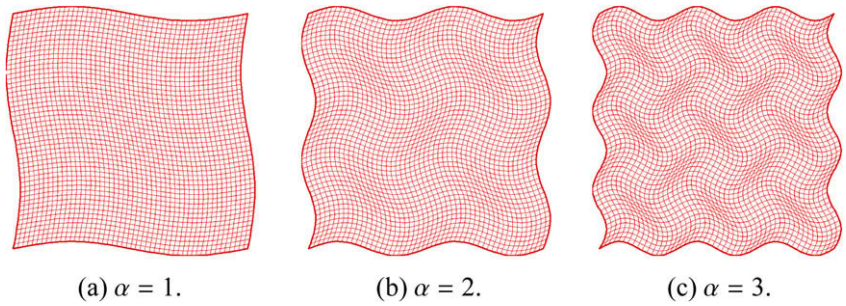

Fig. 7. Computational grid at $\alpha = (1, 2, 3)$ with $MX = MY = 50$.

where $(x_c, y_c) = (26, 51)$. The initial values of f, f_x and f_y are obtained from Eq. (77) and fixed with zero values at the boundary of the computational domain. The time step is $\Delta t = 1.0$. Revolution speed is set so that one revolution is completed after $16MX$ steps. The CFL number at $\Delta t = 1.0$ corresponds to 0.28 in all computations. The spatial velocity profiles imposed by Eq. (78) are:

$$\begin{cases} u = -2\pi(y - y_c)/(16MX) \\ v = -2\pi(x - x_c)/(16MX) \end{cases} \tag{78}$$

Numerical error to the initial profile after one revolution is evaluated by Eq. (20). Figs. 8–10 show the comparison of the numerical error obtained by the CIP–CUV method, the present CIP method and the present CIP method with semi-nonlinear function, respectively. The CIP–CUV method has third-order accuracy with equal-spaced grid ($\alpha = 0$). As α increases, numerical accuracies of the CIP–CUV method reduce to the second order. The CIP–CUV method strongly depends on the mesh shape. Numerical accuracies of case 2D-2 are 2.80, 2.81, 2.81 and 2.77 with $\alpha = 0, 1, 2$ and 3, respectively. Case 2D-2 is highly accurate even when the advection equation is solved on the skewed grid shape with $\alpha = 3$ in spite of the use of the linear coordinate function. As shown in Fig. 10, numerical accuracy of the case 2D-3 method does not depend on the grid spacing when the coordinate function of the semi-nonlinear type is used. Numerical accuracy of case 2D-3 is 2.80, even for the worst case with $\alpha = 0$. Numerical accuracies with $\alpha = 1, 2$ and 3 have accuracies of 2.82, 2.83 and 2.84, respectively, better than that of $\alpha = 0$. Numerical errors with $\alpha = 1, 2$ and 3 approach the result of $\alpha = 0$ as the number of mesh grid points increases. Consequently, those cases have slightly steep gradients. The use of splitting procedure usually deteriorates numerical accuracy. However, the present method maintains higher order accuracy although the first order upwind scheme is applied to the normal direction to that of the advection.

Fig. 11 shows the comparison of the profile after one revolution with the initial shape at $\alpha = 3$ of case 2D-3. The present CIP method preserves the initial shape after one revolution. The present CIP method can solve the advection equations with third-order accuracy over a complicated mesh even though this requires computational costs for the coordinate transformation.

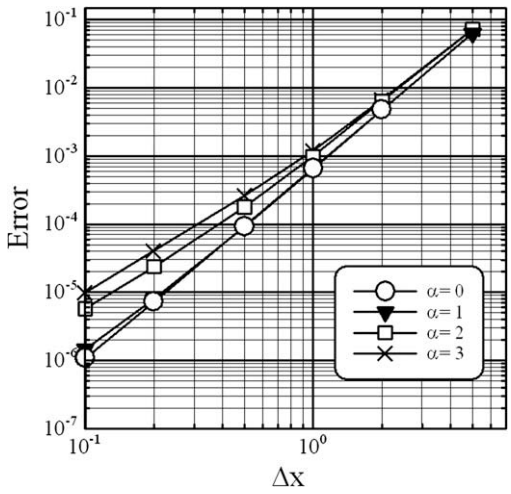

Fig. 8. CIP–CUV method (case 2D-1 by splitting technique).

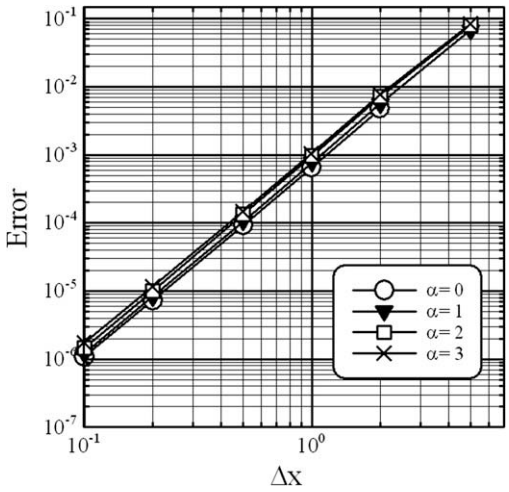

Fig. 9. Present CIP method (case 2D-2 by splitting technique).

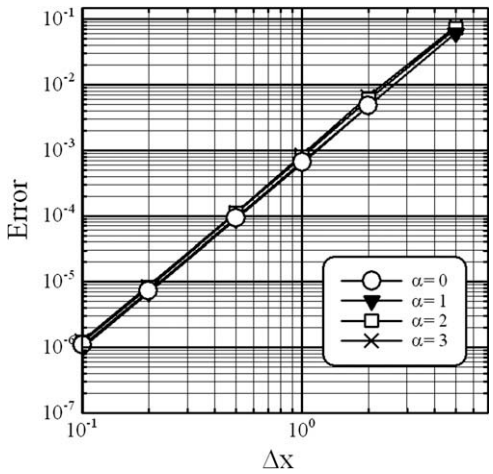

Fig. 10. Present CIP method (case 2D-3 by splitting technique).

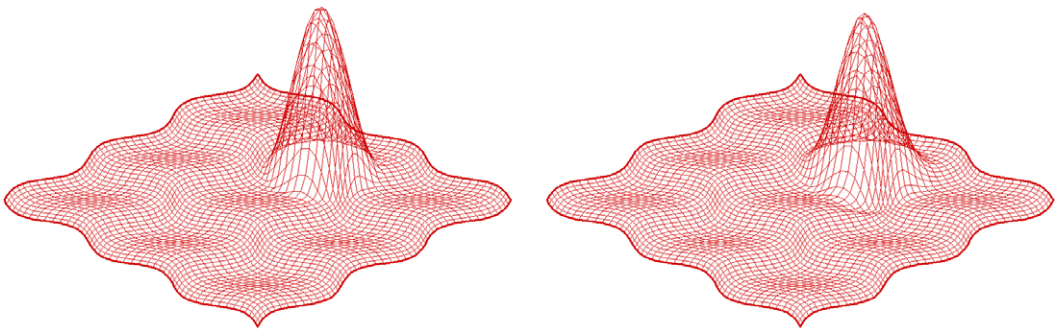

Fig. 11. Solid revolution problem obtained by the present CIP scheme with semi-nonlinear function ($MX = MY = 50$, $\alpha = 3$).

Table 4 shows the comparison of the computational time in the CIP–CUV method and present CIP method. These results are obtained at $MX = MY = 50$ in the solid revolution problem. Cases 2D-2 and 2D-3(1) in the present CIP require an increment of the computational cost of about 5%. In case 2D-3(2), the metrics in the advection phase are computed at every time step. The computational time in that case takes 1.19 times greater than the CIP–CUV method.

Table 4
Comparison of the CIP–CUV and present CIP method in the two-dimensional case.

Case	CIP method	CPU time (s)	Time ratio to the CIP–CUV	Metric in advection
2D-1	CIP–CUV	4.07	1.00	Memorized
2D-2	Present	4.23	1.04	Memorized
2D-3(1)	Present	4.26	1.05	Memorized
2D-3(2)	Present	4.83	1.19	Not memorized

3.3. Extension to multi-dimensional CIP method by direct technique

The present approach is also straightforward to the multi-dimensional CIP method by direct technique. There are some versions of the multi-dimensional CIP method. In the present analysis, we use the B-type CIP method in two dimensions [8]. The B-type CIP method assumes that all the variables (f, f_ξ, f_η) have the continuity at grid points (j, k), $(j+jsign, k)$, $(j, k+ksign)$ and $(j+jsign, k+ksign)$. Each coefficient of the interpolation function is shown in the appendix. In the advection phase, metrics for coordinate transformation are computed from Eq. (69) and the gradient values f_ξ and f_η are transformed by Eq. (68). The differential terms of non-advection phase in Eqs. (72)–(74) are evaluated by the central difference scheme. To demonstrate the efficiency of the present method, some numerical tests in two dimensions are conducted in this section.

At first, we apply the direct technique to solve the solid revolution problem in the previous section and validate the accuracy of the present CIP method by the direct technique. The computational conditions correspond to those in Section 3.2. Figs. 12–14 show the comparison of the numerical error of the case 2D-1, 2D-2 and 2D-3 by the direct technique, respectively. The CIP–CUV method is less than third order accuracy except $\alpha = 0$. The CIP–CUV method has the dependency of the mesh shape. Numerical accuracies of case 2D-2 are 3.00, 3.00, 3.00 and 2.99 with $\alpha = 0, 1, 2$ and 3, respectively. In the case 2D-3, numerical accuracies with $\alpha = 0, 1, 2$ and 3 have accuracies of 3.00, 3.06, 3.07 and 3.00. As shown in Figs. 9 and 10, the numerical accuracies of the splitting technique in the present problem are 2.80, 2.81, 2.81 and 2.77 in the case 2D-2, and 2.80, 2.82, 2.83, and 2.84 in the case 2D-3. The results of the cases 2D-2 and 2D-3 by the direct technique are more accurate than those by the splitting technique. The present method by the direct technique with the semi-nonlinear function maintains the third-order accuracy in all the cases.

Second, we solve Zalesak's solid revolution problem by the splitting and direct techniques. The details of the problem are given in [9]. Fig. 15(a) shows the schematic picture of Zalesak's problem over the wavy grid. The computational grid is created by Eq. (76) with $\alpha = 3.0$ and $MX = MY = 100$. The velocity field on the computational domain is specified as

$$u = -2\pi(y - 50), \quad v = 2\pi(x - 50). \tag{79}$$

The time step is $\Delta t = 1/6400$. Revolution speed is set so that one revolution is completed after 6400 steps. The outer boundary condition is imposed as a free-slip boundary. Figs. 12(c) and 15(b) show the initial profiles and the numerical profiles after one complete revolution. The present method maintains the shape of the initial profile and gives a stable, weakly diffusive but non-monotone result. The present method can easily incorporate the digitizer function [10]. Fig. 15(d) shows the numerical result obtained using the digitizer function. The numerical profile can be maintained sharply. Fig. 15(e) and (f) show the numerical results obtained by the splitting technique. These result by the splitting technique have the asymmetric profiles because of the skewed computational mesh. The profile by the splitting technique is still asymmetric even when the digitizer function is applied.

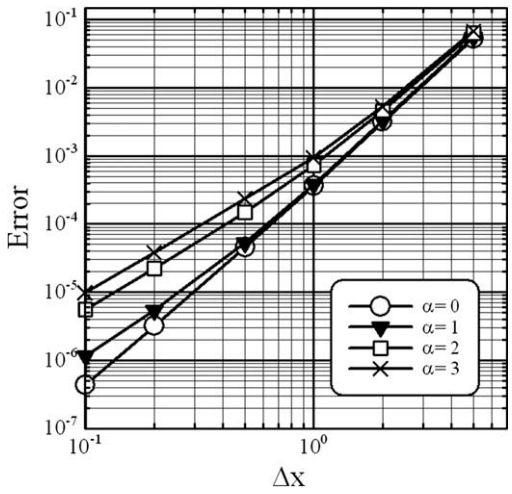

Fig. 12. CIP–CUV method (case 2D-1 by direct technique).

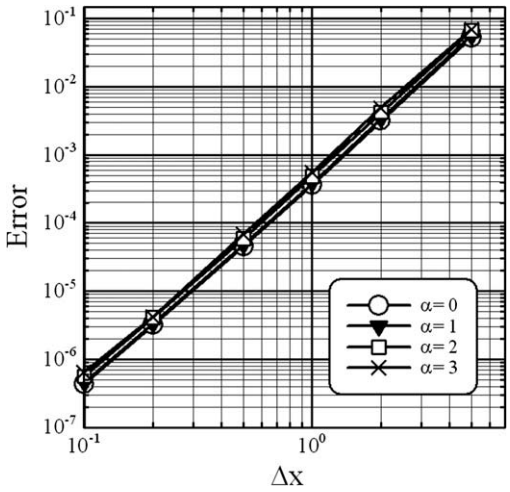

Fig. 13. Present CIP method (case 2D-2 by direct technique).

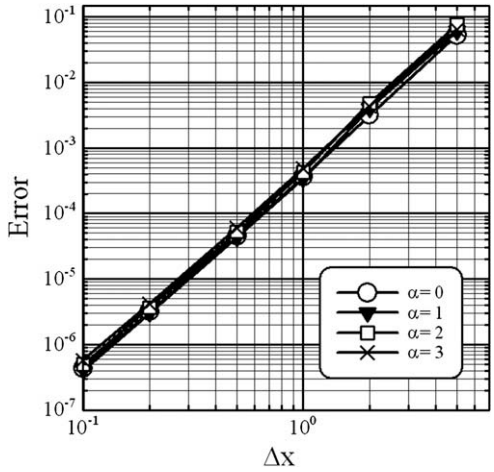

Fig. 14. Present CIP method (case 2D-3 by direct technique).

Next, we apply the present scheme to frontogenesis problem [11] and demonstrate that the scheme provides good results over the wavy grid even if the velocity is strongly fluctuating and more complex. The details of the problem are given by Doswell [12] and the analytical solution is known. In the problem, a circular vortex is assumed and the velocity is given by

$$v_x = -v_T \frac{y}{r} \tag{80}$$

$$v_y = v_T \frac{x}{r} \tag{81}$$

$$v_T(r) = sech^2(r) tanh(r)/v_{T0}. \tag{82}$$

where $r = \sqrt{x^2 + y^2}$ and v_{T0} is a constant which is determined so that maximum value of v_T is equal to unity. The initial condition of f is distributed in the y-direction and given by

$$f = -tanh(y/2). \tag{83}$$

The wavy grid is created by Eq. (84).

$$\begin{aligned} x_0 &= 8(j-1)/(MX-1) - 4 \\ y_0 &= 8(k-1)/(MY-1) - 4 \\ x_{j,k} &= x_0 + 0.3sin(2\pi\alpha y_0) \\ y_{j,k} &= y_0 + 0.3sin(2\pi\alpha x_0) \end{aligned} \tag{84}$$

where $\alpha = 3$. $\alpha = 0$ corresponds to the orthogonal grid. In the computations, $MX = MY = 60$. The numerical tests are performed with the $CFL = 0.4$. The numerical result of the present scheme by the direct technique, that by the splitting technique and the analytical result are shown in Fig. 16. The coordinate function in the present scheme uses the semi-nonlinear

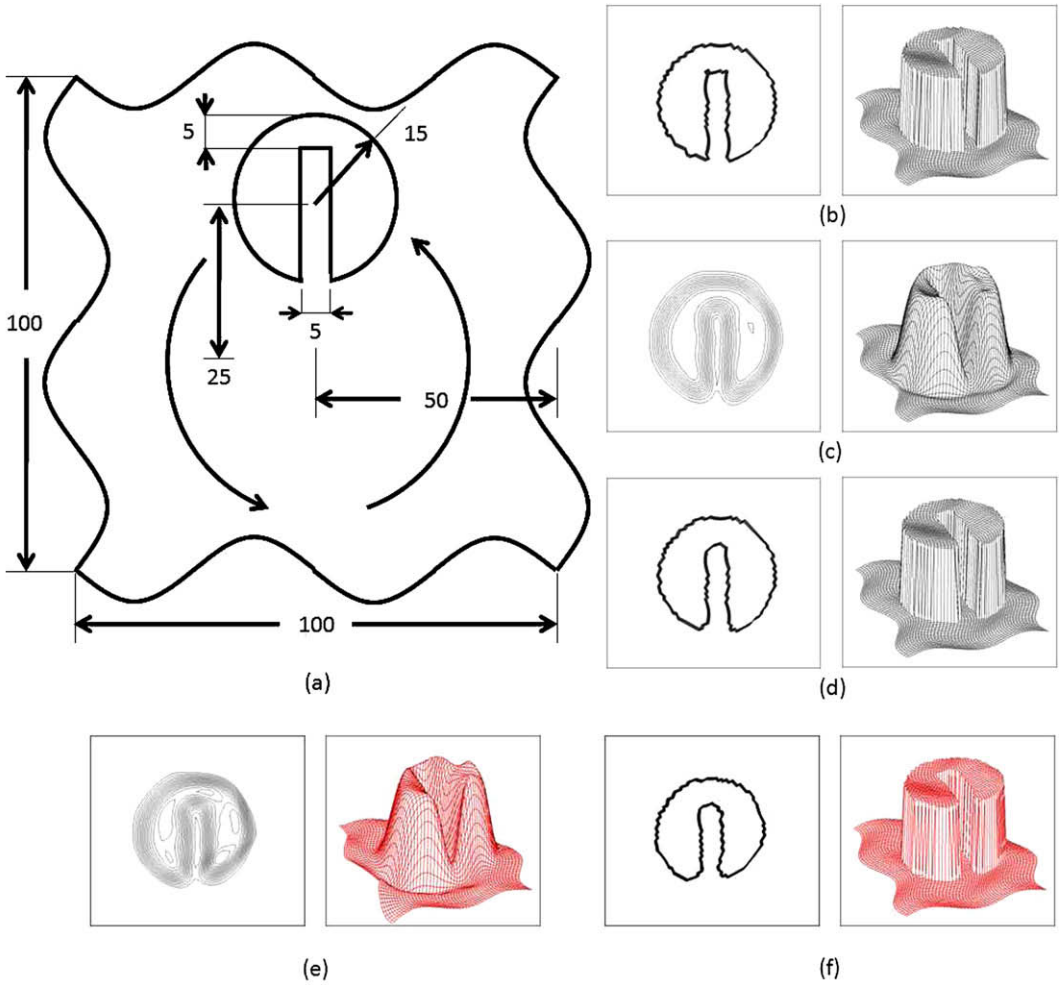

Fig. 15. (a) Schematic picture of Zalesak's problem over the wavy grid. The value of f inside a cut-out cylinder is 1.0, while outside $f = 0.0$. Contour plots and three-dimensional views of the profile of f: (b) Initial profiles, (c) the numerical result after one revolution by the direct technique,(d) the numerical result after one revolution by the direct technique with the digitizer function, (e) the numerical result after one revolution by the splitting technique and (f) the numerical result after one revolution by the splitting technique with the digitizer function.

function. Although the computational grid has the wavy form, the numerical result by the directional technique is in good agreement with the analytical solution. The numerical result by the splitting technique can not capture the details of the vortex motion because the splitting technique deteriorates the numerical accuracy rather than that of the direct technique in general. The numerical results of the three test problem show that the direct technique is more effective to accurately capture the flowfield than the splitting technique.

The curvilinear coordinates are often employed to resolve flows near boundaries. In general, fine meshes are placed around the boundaries. We construct mesh with large aspect ratio in order to investigate the capability of the present method on the different mesh size. The mesh system is defined as

$$
\begin{aligned}
x_{r,j} &= 1 + \beta sin(\gamma\pi(j-1)/(MX-1)) \\
y_{r,k} &= 1 + \beta sin(\gamma\pi(k-1)/(MY-1)) \\
x0_j &= \sum_{n=1}^{j} x_{r,n} \Big/ \sum_{n=1}^{MX} x_{r,n} \\
y0_k &= \sum_{n=1}^{k} y_{r,n} \Big/ \sum_{n=1}^{MY} y_{r,n} \\
\theta_j &= 2\pi\alpha(x0_j + C_x) \\
\theta_k &= 2\pi\alpha(y0_k + C_y) \\
x_{j,k} &= L_x\left[x0_j + C_x + 0.03sin(\theta_k)\right] \\
y_{j,k} &= L_y\left[y0_k + C_y + 0.03sin(\theta_j)\right]
\end{aligned}
\tag{85}
$$

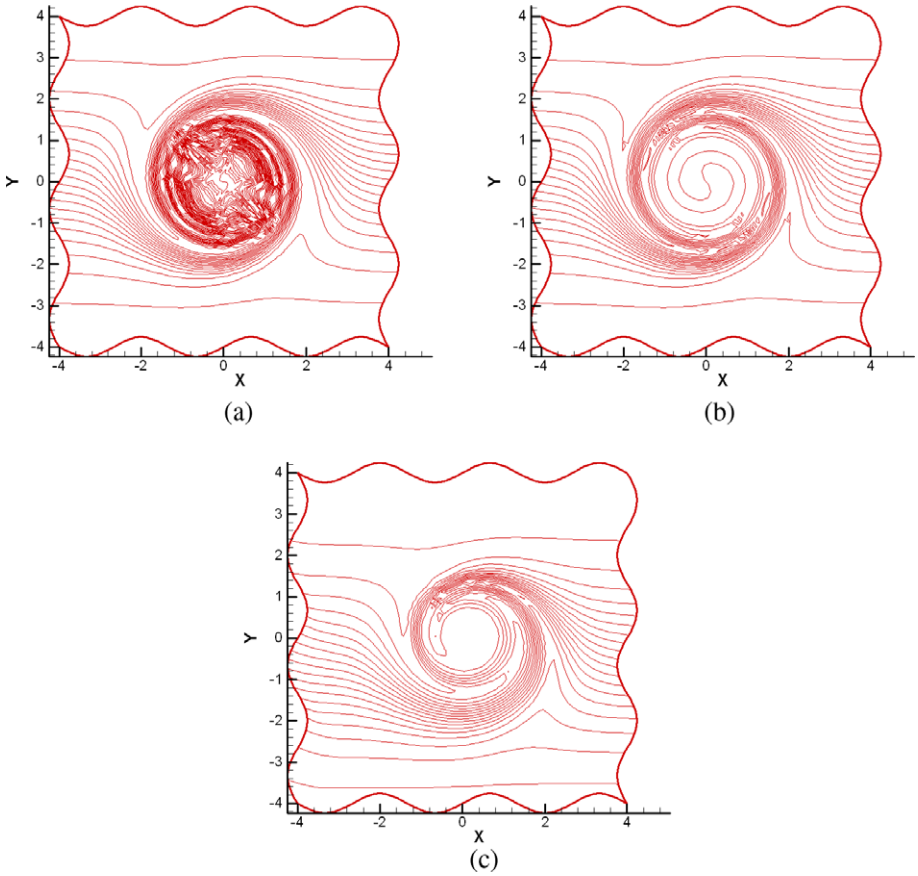

Fig. 16. (a) analytic solution ($\alpha = 3$), (b) the numerical result by the direct technique ($\alpha = 3$) and (c) the numerical result by the splitting technique ($\alpha = 3$).

where α, β and γ are the parameters for wavy shape; C_x and C_y are the grid parameters; L_x and L_y are size of the computational domain. We again solve Zalesak's problem and frontogenesis problem. $L_x = L_y = 100$, $C_x = C_y = 0.0$ and $MX = MY = 100$ are set in Zalesak's problem. The velocity profile in Zalesak's problem is specified by Eq. (79). Those of frontogenesis problem are defined as $L_x = L_y = 8$, $C_x = C_y = 0.5$ and $MX = MY = 60$. Eqs. (80), (81) and (82) are assumed as the velocity field in the frontogenesis problem. In each test, $\alpha = 3.0$, $\beta = 0.9$ and $\gamma = 7.0$. The aspect ratio of the computational grid corresponds to about 20 in maximum. Fig. 17 shows the computational grid used in these test problems. We apply the case 2D-3 by direct technique based on the type-B CIP method. The coordinate function is semi-nonlinear function.

Fig. 18 shows the contour plots and three-dimensional view of the numerical profile in Zalesak's problem. The analytical result and the numerical results of the present scheme are shown in Fig. 18(a) and (b), respectively. The numerical profile in Fig. 18(b) losts the key hole of the solid body because the density of the mesh severely changes in the computational domain. Fig. 18(c) shows the numerical result with the digitizer function. The numerical profile finely maintains the initial shape over the mesh.

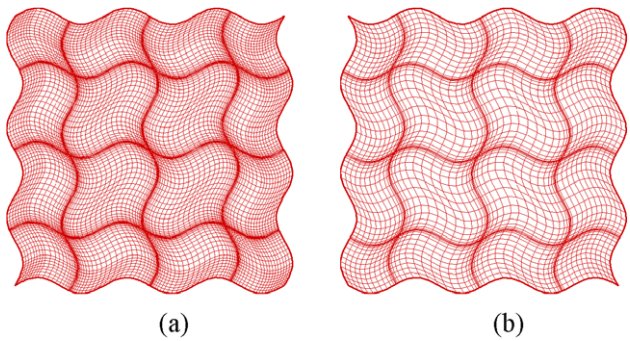

Fig. 17. Wavy grid: (a) Zalesak's problem ($MX = MY = 100$). (b) frontogenesis problem ($MX = MY = 60$).

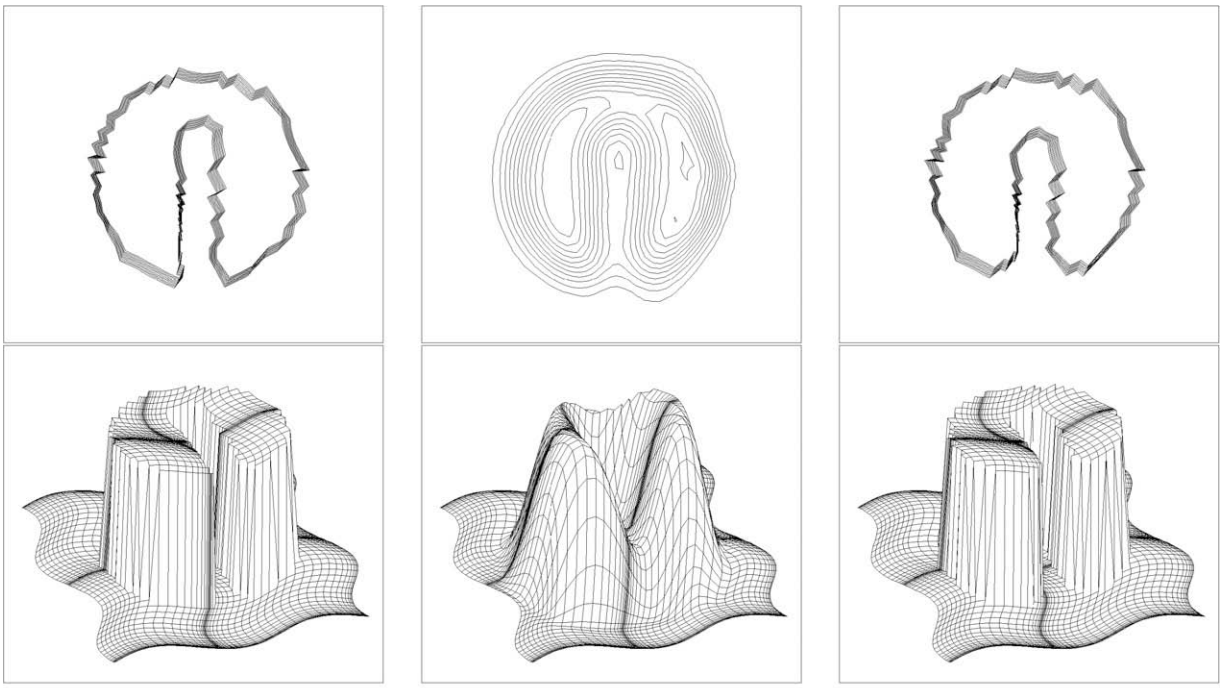

Fig. 18. Contour plots (above) and three-dimensional views (below): (a) initial profile. (b) The numerical result after one revolution. (c) The numerical result after one revolution with the digitizer function.

Fig. 19 represents the numerical results of the frontogenesis problem. From comparison with the analytic solution in Fig. 19(a), the numerical result (Fig. 19(b)) agrees well with the theoretical one. The scheme can stably capture the fine structure even wavy grid with the different mesh size.

3.4. Extension to three dimensions

Once the two-dimensional scheme is established, it is straightforward to extend our method to three dimensions. The advection equation in three dimensions can be written as follows:

$$\frac{\partial f}{\partial t}+\frac{\partial (uf)}{\partial x}+\frac{\partial (vf)}{\partial y}+\frac{\partial (wf)}{\partial z}=0 \tag{86}$$

$$\frac{\partial f}{\partial t}+u\frac{\partial f}{\partial x}+v\frac{\partial f}{\partial y}+w\frac{\partial f}{\partial z}=-f\left(\frac{\partial u}{\partial x}+\frac{\partial v}{\partial y}+\frac{\partial w}{\partial z}\right) \tag{87}$$

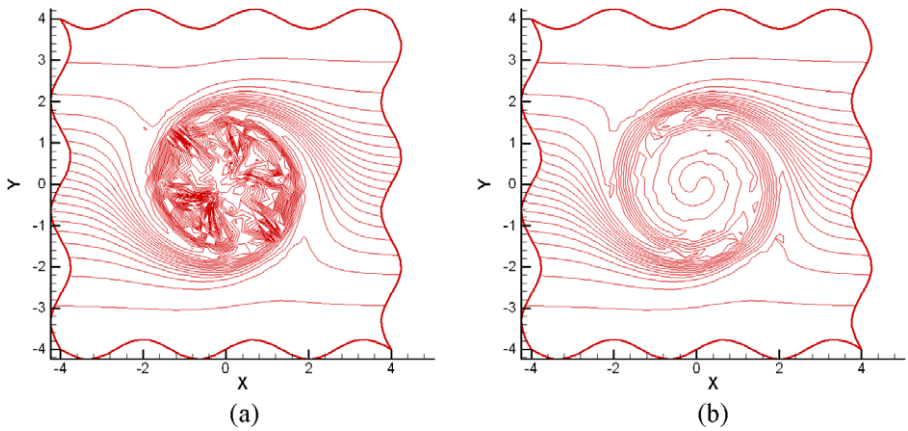

Fig. 19. (a) Analytic solution and (b) the numerical result.

When Eq. (87) is rewritten on the curvilinear coordinates,

$$\frac{\partial f}{\partial t}+U\frac{\partial f}{\partial \xi}+V\frac{\partial f}{\partial \eta}+W\frac{\partial f}{\partial \zeta}=H \tag{88}$$
$$H=-f\left(\xi_x\frac{\partial u}{\partial \xi}+\eta_x\frac{\partial u}{\partial \eta}+\zeta_x\frac{\partial u}{\partial \zeta}+\xi_y\frac{\partial v}{\partial \xi}+\eta_y\frac{\partial v}{\partial \eta}+\zeta_y\frac{\partial v}{\partial \zeta}+\xi_z\frac{\partial w}{\partial \xi}+\eta_z\frac{\partial w}{\partial \eta}+\zeta_z\frac{\partial w}{\partial \zeta}\right)$$

where $U=\xi_x u+\xi_y v+\xi_z w,\ V=\eta_x u+\eta_y v+\eta_z w$ and $W=\zeta_x u+\zeta_y v+\zeta_z w$.

The gradient advection equation can be derived in the same manner as in the one-dimensional case. We take the differentiations of Eq. (88) for $\xi,\ \eta$ and ζ.

$$\frac{\partial f_\xi}{\partial t}+U\frac{\partial f_\xi}{\partial \xi}+V\frac{\partial f_\xi}{\partial \eta}+W\frac{\partial f_\xi}{\partial \zeta}=H_\xi-\left(U_\xi\frac{\partial f}{\partial \xi}+V_\xi\frac{\partial f}{\partial \eta}+W_\xi\frac{\partial f}{\partial \zeta}\right) \tag{89}$$
$$\frac{\partial f_\eta}{\partial t}+U\frac{\partial f_\eta}{\partial \xi}+V\frac{\partial f_\eta}{\partial \eta}+W\frac{\partial f_\eta}{\partial \zeta}=H_\eta-\left(U_\eta\frac{\partial f}{\partial \xi}+V_\eta\frac{\partial f}{\partial \eta}+W_\eta\frac{\partial f}{\partial \zeta}\right) \tag{90}$$
$$\frac{\partial f_\zeta}{\partial t}+U\frac{\partial f_\zeta}{\partial \xi}+V\frac{\partial f_\zeta}{\partial \eta}+W\frac{\partial f_\zeta}{\partial \zeta}=H_\zeta-\left(U_\zeta\frac{\partial f}{\partial \xi}+V_\zeta\frac{\partial f}{\partial \eta}+W_\zeta\frac{\partial f}{\partial \zeta}\right) \tag{91}$$

Eqs. (89)–(91) are split into the advection and the non-advection equations. In the same manner as in the one-dimensional and the two-dimensional cases, the advection equations are solved on the curvilinear coordinates and the non-advection equations on the physical coordinates. First, the numerical profiles of $f, f_\xi,\ f_\eta$ and f_ζ are computed by the present CIP method.

Advection equations for the present CIP method

$$\frac{\partial f_\xi}{\partial t}+U\frac{\partial f_\xi}{\partial \xi}+V\frac{\partial f_\xi}{\partial \eta}+W\frac{\partial f_\xi}{\partial \zeta}=0 \tag{92}$$
$$\frac{\partial f_\eta}{\partial t}+U\frac{\partial f_\eta}{\partial \xi}+V\frac{\partial f_\eta}{\partial \eta}+W\frac{\partial f_\eta}{\partial \zeta}=0 \tag{93}$$
$$\frac{\partial f_\zeta}{\partial t}+U\frac{\partial f_\zeta}{\partial \xi}+V\frac{\partial f_\zeta}{\partial \eta}+W\frac{\partial f_\zeta}{\partial \zeta}=0 \tag{94}$$

Non-advection equations for the present CIP method

In the present CIP method, the non-advection equations on the physical coordinates are projected and solved to the curvilinear coordinates.

$$\frac{\partial f}{\partial t}=H \tag{95}$$

Take the differentiations of Eq. (95) to derivate the non-advection equations on the gradient values for the physical coordinates.

$$\frac{\partial f_x}{\partial t}=H_x-\frac{\partial u}{\partial x}f_x+\frac{\partial v}{\partial x}f_y+\frac{\partial w}{\partial x}f_z \tag{96}$$
$$\frac{\partial f_y}{\partial t}=H_y-\frac{\partial u}{\partial y}f_x+\frac{\partial v}{\partial y}f_y+\frac{\partial w}{\partial y}f_z \tag{97}$$
$$\frac{\partial f_y}{\partial t}=H_z-\frac{\partial u}{\partial z}f_x+\frac{\partial v}{\partial z}f_y+\frac{\partial w}{\partial z}f_z \tag{98}$$

The spatial derivatives in the equations are transformed to curvilinear coordinates using the chain rule when solving the non-advection phase.

$$\begin{aligned}\frac{\partial H}{\partial x}&=\xi_x\frac{\partial H}{\partial \xi}+\eta_x\frac{\partial H}{\partial \eta}+\zeta_x\frac{\partial H}{\partial \zeta}\\ \frac{\partial H}{\partial y}&=\xi_y\frac{\partial H}{\partial \xi}+\eta_y\frac{\partial H}{\partial \eta}+\zeta_y\frac{\partial H}{\partial \zeta}\\ \frac{\partial H}{\partial z}&=\xi_z\frac{\partial H}{\partial \xi}+\eta_z\frac{\partial H}{\partial \eta}+\zeta_z\frac{\partial H}{\partial \zeta}\end{aligned} \tag{99}$$

The spatial differentiations of the velocities are also computed using the differential chain rule as for Eq. (99) (H is replaced by u, v or w). The metrics in the non-advection phase are evaluated by the second order central difference scheme in the same manner as the one-dimensional and the two-dimensional cases.

In the present paper, we use the type-A scheme to solve the three-dimensional problems [8]. The type-A scheme can be written as Eq. (100). These coefficients of the interpolation function and the metrics for coordinate transformation are shown in the appendix. The directional splitting technique can be easily extended to three dimensions as denoted in Section 3.2.

$$
\begin{aligned}
F_{j,k,l}(\xi,\eta,\zeta) = {} & [(B1_{j,k,l}\xi + B2_{j,k,l}\eta + B3_{j,k,l}\zeta + B4_{j,k,l})\xi + B5_{j,k,l}\eta + \partial_\xi f_{j,k,l}]\xi \\
& + [(B6_{j,k,l}\eta + B7_{j,k,l}\zeta + B8_{j,k,l}\xi + B9_{j,k,l})\eta + B10_{j,k,l}\zeta + \partial_\eta f_{j,k,l}]\eta \\
& + [(B11_{j,k,l}\zeta + B12_{j,k,l}\xi + B13_{j,k,l}\eta + B14_{j,k,l})\zeta + B15_{j,k,l}\xi + \partial_\zeta f_{j,k,l}]\zeta \\
& + B16_{j,k,l}\xi\eta\zeta + f_{j,k,l}
\end{aligned} \tag{100}
$$

In order to evaluate the three-dimensional solver, the present scheme is applied to the problem of three-dimensional solid-body rotation [13]. The velocity vector $\vec{v} = (u, v, w)$ is set as

$$\vec{v} = \vec{\omega} \times \vec{r} \tag{101}$$

where $\vec{r} = (x, y, z)$ and $\vec{\omega} = 2\pi/\sqrt{2}(0, -1, 1)$. The time step is imposed to satisfy $CFL \leqslant 0.2$ in all grid points. We use the mesh with $MX = MY = MZ = 100$ defined by Eq. (102). The center of the solid body is located at $(x, y, z) = (0, 20, 20)$.

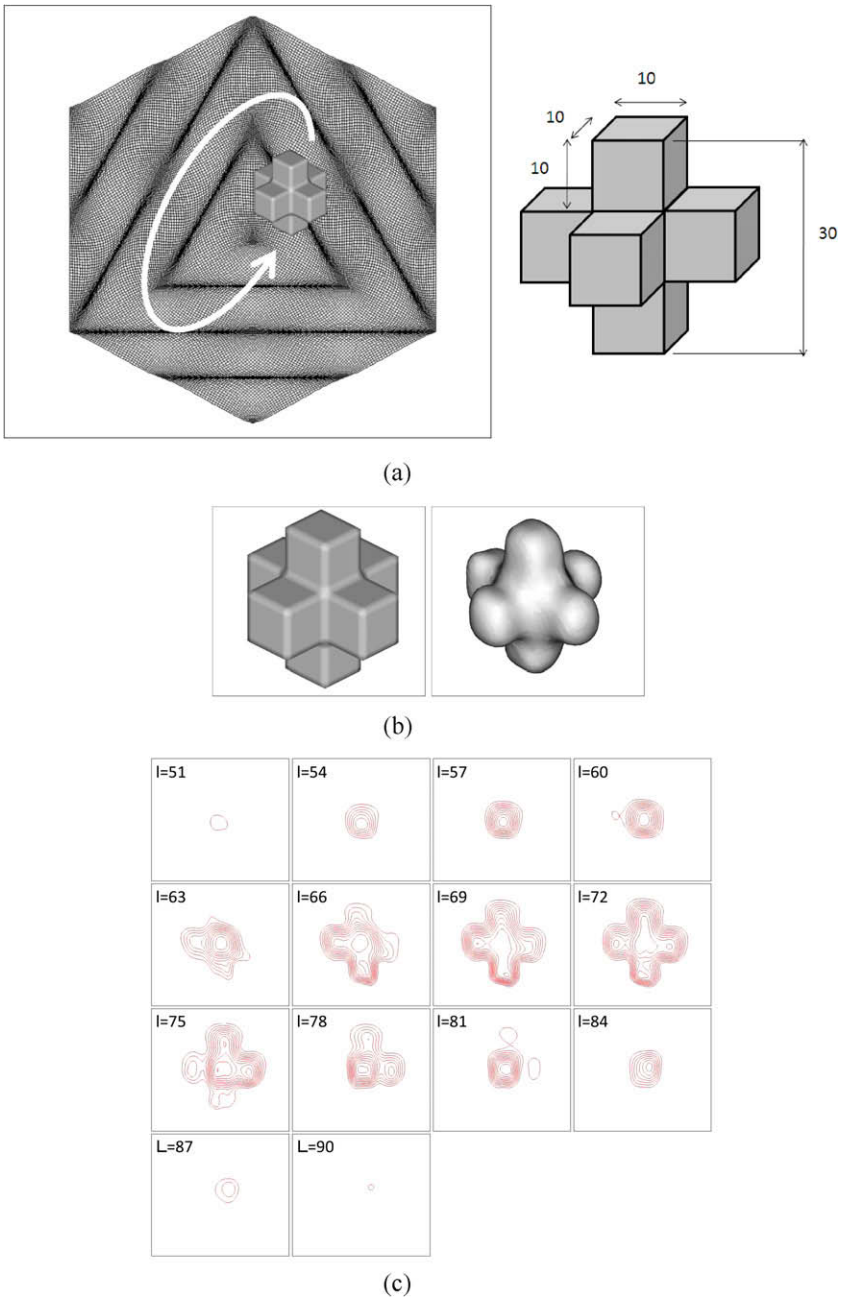

Fig. 20. (a) Schematic picture of the three-dimensional solid rotation problem. At the boundary and inside the rigid body, the value of f is set to 1.0, while $f = 0.0$ outside. (b) Initial shape. (c) The numerical result after one revolution.

$$
\begin{aligned}
x_0 &= (j-1)/(MX-1) - 1/2 \\
y_0 &= (k-1)/(MY-1) - 1/2 \\
z_0 &= (l-1)/(MZ-1) - 1/2 \\
x_{j,k,l} &= 100(x_0 + 0.03sin(2\alpha\pi(y_0+z_0))) \\
y_{j,k,l} &= 100(y_0 + 0.03sin(2\alpha\pi(z_0+x_0))) \\
z_{j,k,l} &= 100(z_0 + 0.03sin(2\alpha\pi(x_0+y_0)))
\end{aligned} \tag{102}
$$

Fig. 20(a) shows the schematic picture of this problem. Fig. 20(b) shows an isosurface of $f = 0.5$ for the initial shape and the numerical result. Fig. 20(c) shows the contour plots of f with the $l = const.$ plane at $t = 1.0$. The contour plots are drawn from 0.1 to 1.2 with increments of 0.1. The present scheme maintains the initial profile finely.

4. Conclusions

We investigated the problems of the CIP method on curvilinear coordinates and improved the method to solve the advection equation accurately. The proposed method takes different numerical procedures on the gradient value in contrast to the original CIP method on curvilinear coordinates. In the advection phase, the gradient values on the curvilinear coordinates are obtained from those values on the physical coordinates and those metrics. The metrics in the advection phase are computed using stencils in the CIP method. The original CIP method and the present CIP method on curvilinear coordinates can maintain consistency only when these conditions are satisfied. In the non-advection phase, those equations based on the physical coordinates are extended to curvilinear coordinates and are solved by arbitrary schemes. The present method needs two types of metrics for coordinate transformation in the advection and non-advection phases. The present CIP method can easily apply to the splitting technique and the direct multi-dimensional technique and solve the advection equation accurately.

Acknowledgment

We appreciate the three anonymous referees for their constructive suggestions and kind advice for the improvement of the original manuscript. We also appreciate the editors for their kindness.

Appendix A

Here, we summarize the coefficients of the type-B scheme in the two dimensions and the type-A scheme in the three dimensions over the curvilinear coordinates.

A.1. Type-B scheme in the two dimensions

$$
\begin{aligned}
F_{j,k}(\xi,\eta) = {} & A1_{j,k}\xi^3 + A2_{j,k}\xi^2 + \partial_\xi f_{j,k}\xi + A3_{j,k}\eta^3 + A4_{j,k}\eta^2 + \partial_\eta f_{j,k}\eta \\
& + A5_{j,k}\xi^2\eta + A6_{j,k}\xi\eta + A7_{j,k}\xi\eta^2 + A8\xi^3\eta + A9\xi\eta^3 + f_{j,k}
\end{aligned} \tag{103}
$$

$$
\begin{aligned}
A1_{j,k} &= \frac{-2(f_{j+1,k} - f_{j,k}) + (f_{\xi j+1,k} + f_{\xi j,k})\Delta\xi}{\Delta\xi^3} \\
A2_{j,k} &= \frac{3(f_{j+1,k} - f_{j,k}) - 2(f_{\xi j+1,k} + f_{\xi j,k})\Delta\xi}{\Delta\xi^2} \\
A3_{j,k} &= \frac{-2(f_{j,k+1} - f_{j,k}) + (f_{\eta j,k+1} + f_{\eta j,k})\Delta\eta}{\Delta\eta^3} \\
A4_{j,k} &= \frac{3(f_{j,k+1} - f_{j,k}) - 2(f_{\eta j,k+1} + f_{\eta j,k})\Delta\eta}{\Delta\eta^2} \\
A5_{j,k} &= \frac{-3(f_{j+1,k+1} + f_{j+1,k} - f_{j,k+1} - f_{j,k}) - 2(f_{\xi j,k+1} - f_{\xi j,k})\Delta\xi - (f_{\xi j+1,k+1} - f_{\xi j+1,k})\Delta\xi}{\Delta\xi^2\eta} \\
A6_{j,k} &= \frac{-(f_{j,k} - f_{j+1,k} + f_{j+1,k+1} - f_{j,k+1}) + (f_{\xi j,k+1} - f_{\xi j,k})\Delta\xi + (f_{\eta j+1,k} - f_{\eta j,k})\Delta\eta}{\Delta\xi\Delta\eta} \\
A7_{j,k} &= \frac{-3(f_{j+1,k+1} + f_{j+1,k} - f_{j,k+1} - f_{j,k}) - 2(f_{\eta j,k+1} - f_{\eta j,k})\Delta\eta - (f_{\eta j+1,k+1} - f_{\eta j+1,k})\Delta\eta}{\Delta\xi\eta^2} \\
A8_{j,k} &= \frac{-2(f_{j,k} - f_{j+1,k} + f_{j+1,k+1} - f_{j,k+1}) - (f_{\xi j,k} + f_{\xi j+1,k} - f_{\xi j+1,k+1} - f_{\xi j+1,k})\Delta\xi}{\Delta\xi^3\Delta\eta} \\
A9_{j,k} &= \frac{-2(f_{j,k} - f_{j+1,k} + f_{j+1,k+1} - f_{j,k+1}) - (f_{\eta j,k} - f_{\eta j+1,k} - f_{\eta j+1,k+1} - f_{\eta j,k+1})\Delta\eta}{\Delta\xi\Delta\eta^3} \\
A10_{j,k} &= \frac{-2(f_{j,k} - f_{j+1,k} + f_{j+1,k+1} - f_{j,k+1}) - (f_{\eta j,k} - f_{\eta j+1,k} - f_{\eta j+1,k+1} + f_{\eta j,k+1})\Delta\eta}{\Delta\xi\Delta\eta^3}
\end{aligned}
$$

where $\xi = -U_{j,k}\Delta t,\ \eta = -V_{j,k}\Delta t$. Here, $U = \xi_x u + \xi_y v,\ V = \eta_x u + \eta_y v$.

Metrics for coordinate transformation are computed from Eq. (69). Depending on the sign of U and V, we must change the subscript of the coefficients $A1_{j,k}$ to $A10_{j,k}$: $j+1 \to j-1$ and $\Delta\xi \to -\Delta\xi$ for $U \geqslant 0$ and $k+1 \to k-1$ and $\Delta\eta \to -\Delta\eta$ for $V \geqslant 0$.

A.2. Type-A scheme in the three dimensions

$$\begin{aligned}
F_{j,k,l}(\xi,\eta,\zeta) &= [(B1_{j,k,l}\xi + B2_{j,k,l}\eta + B3_{j,k,l}\zeta + B4_{j,k,l})\xi + B5_{j,k,l}\eta + \partial_\xi f_{j,k,l}]\xi \\
&+ [(B6_{j,k,l}\eta + B7_{j,k,l}\zeta + B8_{j,k,l}\xi + B9_{j,k,l})\eta + B10_{j,k,l}\zeta + \partial_\eta f_{j,k,l}]\eta \\
&+ [(B11_{j,k,l}\zeta + B12_{j,k,l}\xi + B13_{j,k,l}\eta + B14_{j,k,l})\zeta + B15_{j,k,l}\xi + \partial_\zeta f_{j,k,l}]\zeta \\
&+ B16_{j,k,l}\xi\eta\zeta + f_{j,k,l}
\end{aligned} \tag{104}$$

where $\xi = -U_{j,k,l}\Delta t,\ \eta = -V_{j,k,l}\Delta t$ and $\zeta = -W_{j,k,l}\Delta t$. Here, $U = \xi_x u + \xi_y v + \xi_z w,\ V = \eta_x u + \eta_y v + \eta_z w$ and $W = \zeta_x u + \zeta_y v + \zeta_z w$.

$$\begin{aligned}
B1_{j,k,l} &= [-2D_j + \partial_\xi(f_{j,k,l} + f_{j+1,k,l})\Delta\xi]/\Delta\xi^3 \\
B2_{j,k,l} &= -[B17_{j,k,l} + \partial_\xi D_j\Delta\xi]/\Delta\xi^2\Delta\eta \\
B3_{j,k,l} &= -[B18_{j,k,l} + \partial_\xi D_k\Delta\xi]/\Delta\xi^2\Delta\zeta \\
B4_{j,k,l} &= [3D_j - \partial_\xi(f_{j+1,k,l} + 2f_{j,k,l})\Delta\xi]/\Delta\xi^2 \\
B5_{j,k,l} &= [B17_{j,k,l} + \partial_\xi D_k\Delta\xi + \partial_\eta D_j\Delta\eta]/\Delta\xi\Delta\eta \\
B6_{j,k,l} &= [-2D_k + \partial_\eta(f_{j,k,l} + f_{j,k+1,l})\Delta\eta]/\Delta\eta^3 \\
B7_{j,k,l} &= -[B19_{j,k,l} + \partial_\eta D_k\Delta\eta]/\Delta\eta^2\Delta\zeta \\
B8_{j,k,l} &= -[B17_{j,k,l} + \partial_\eta D_j\Delta\eta]/\Delta\xi\Delta\eta^2 \\
B9_{j,k,l} &= [3D_k - \partial_\eta(f_{j,k+1,l} + 2f_{j,k,l})\Delta\eta]/\Delta\eta^2 \\
B10_{j,k,l} &= [B19_{j,k,l} + \partial_\eta D_k\Delta\eta + \partial_\zeta D_j\Delta\zeta]/\Delta\eta\Delta\zeta \\
B11_{j,k,l} &= [-2D_l + \partial_\zeta(f_{j,k,l} + f_{j,k,l+1})\Delta\zeta]/\Delta\zeta^3 \\
B12_{j,k,l} &= -[B18_{j,k,l} + \partial_\zeta D_j\Delta\zeta]/\Delta\xi\Delta\zeta^2 \\
B13_{j,k,l} &= -[B19_{j,k,l} + \partial_\zeta D_j\Delta\zeta]/\Delta\eta\Delta\zeta^2 \\
B14_{j,k,l} &= [3D_l - \partial_\zeta(f_{j,k,l+1} + 2f_{j,k,l})\Delta\zeta]/\Delta\zeta^2 \\
B15_{j,k,l} &= [B18_{j,k,l} + \partial_\zeta D_j\Delta\zeta + \partial_\xi D_k\Delta\xi]/\Delta\xi\Delta\zeta \\
B16_{j,k,l} &= [B17_{j,k,l} + f_{j,k,l+1} - f_{j,k+1,l+1} - f_{j+1,k,l+1} + f_{j+1,k+1,l+1}]/\Delta\xi\Delta\eta\Delta\zeta
\end{aligned}$$

where $D_j = f_{j+1,k,l} - f_{j,k,l},\ D_k = f_{j,k+1,l} - f_{j,k,l},\ D_l = f_{j,k,l+1} - f_{j,k,l}$ and

$$\begin{aligned}
B17_{j,k,l} &= -f_{j,k,l} + f_{j+1,k,l} + f_{j,k+1,l} - f_{j+1,k+1,l} \\
B18_{j,k,l} &= -f_{j,k,l} + f_{j+1,k,l} + f_{j,k,l+1} - f_{j+1,k,l+1} \\
B19_{j,k,l} &= -f_{j,k,l} + f_{j,k+1,l} + f_{j,k,l+1} - f_{j,k+1,l+1}
\end{aligned}$$

Before computing the advection phase, the gradient values on the curvilinear coordinate are calculated by the coordinate transformation.

$$\begin{pmatrix} \tilde{f}_\xi \\ \tilde{f}_\eta \\ \tilde{f}_\zeta \end{pmatrix} = \begin{pmatrix} \tilde{x}_\xi & \tilde{y}_\xi & \tilde{z}_\xi \\ \tilde{x}_\eta & \tilde{y}_\eta & \tilde{z}_\eta \\ \tilde{x}_\zeta & \tilde{y}_\zeta & \tilde{z}_\zeta \end{pmatrix} \begin{pmatrix} f_x \\ f_y \\ f_z \end{pmatrix}$$

Metrics for coordinate transform in three dimensions are computed as

$$\begin{aligned}
&\tilde{x}_\xi = (x_{j+1,k,l} - x_{j,k,l})/\Delta\xi, \tilde{x}_\eta = (x_{j,k+1,l} - x_{j,k,l})/\Delta\eta, \tilde{x}_\zeta = (x_{j,k,l+1} - x_{j,k,l})/\Delta\zeta \\
&\tilde{y}_\xi = (y_{j+1,k,l} - y_{j,k,l})/\Delta\xi, \tilde{y}_\eta = (y_{j,k+1,l} - y_{j,k,l})/\Delta\eta, \tilde{y}_\zeta = (y_{j,k,l+1} - y_{j,k,l})/\Delta\zeta \\
&\tilde{z}_\xi = (z_{j+1,k,l} - z_{j,k,l})/\Delta\xi, \tilde{z}_\eta = (z_{j,k+1,l} - z_{j,k,l})/\Delta\eta, \tilde{z}_\zeta = (z_{j,k,l+1} - z_{j,k,l})/\Delta\zeta \\
&\widetilde{J} = \frac{1}{\tilde{x}_\xi(\tilde{y}_\eta\tilde{z}_\zeta - \tilde{y}_\zeta\tilde{z}_\eta) + \tilde{x}_\eta(\tilde{y}_\zeta\tilde{z}_\xi - \tilde{y}_\xi\tilde{z}_\zeta) + \tilde{x}_\zeta(\tilde{y}_\xi\tilde{z}_\eta - \tilde{y}_\eta\tilde{z}_\xi)}
\end{aligned}$$

The gradient values advanced by the present CIP scheme are inversely transformed to the values in the physical domain when the non-advection phase is solved.

$$\begin{pmatrix} f_x \\ f_y \\ f_z \end{pmatrix} = \begin{pmatrix} \tilde{\xi}_x & \tilde{\xi}_y & \tilde{\xi}_z \\ \tilde{\eta}_x & \tilde{\eta}_y & \tilde{\eta}_z \\ \tilde{\zeta}_x & \tilde{\zeta}_y & \tilde{\zeta}_z \end{pmatrix} \begin{pmatrix} \tilde{f}_\xi \\ \tilde{f}_\eta \\ \tilde{f}_\zeta \end{pmatrix}$$

Metrics for the inverse transformation in three dimensions are calculated as

$$\tilde{\xi}_x = \widetilde{J}(\tilde{y}_\eta \tilde{z}_\zeta - \tilde{y}_\zeta \tilde{z}_\eta), \tilde{\xi}_y = \widetilde{J}(\tilde{z}_\eta \tilde{x}_\zeta - \tilde{z}_\zeta \tilde{x}_\eta), \tilde{\xi}_z = \widetilde{J}(\tilde{x}_\eta \tilde{y}_\zeta - \tilde{x}_\zeta \tilde{y}_\eta)$$
$$\tilde{\eta}_x = \widetilde{J}(\tilde{y}_\zeta \tilde{z}_\xi - \tilde{y}_\xi \tilde{z}_\zeta), \tilde{\eta}_y = \widetilde{J}(\tilde{z}_\zeta \tilde{x}_\xi - \tilde{z}_\xi \tilde{x}_\zeta), \tilde{\eta}_z = \widetilde{J}(\tilde{x}_\zeta \tilde{y}_\xi - \tilde{x}_\xi \tilde{y}_\zeta)$$
$$\tilde{\zeta}_x = \widetilde{J}(\tilde{y}_\xi \tilde{z}_\eta - \tilde{y}_\eta \tilde{z}_\xi), \tilde{\zeta}_y = \widetilde{J}(\tilde{z}_\xi \tilde{x}_\eta - \tilde{z}_\eta \tilde{x}_\xi), \tilde{\zeta}_z = \widetilde{J}(\tilde{x}_\xi \tilde{y}_\eta - \tilde{x}_\eta \tilde{y}_\xi)$$

Depending on the sign of U, V and W, we must change the subscript of the coefficients $B1_{j,k,l}$ to $B16_{j,k,l}$: $j+1 \to j-1$ and $\Delta\xi \to -\Delta\xi$ for $U \geqslant 0$, $k+1 \to k-1$ and $\Delta\eta \to -\Delta\eta$ for $V \geqslant 0$ and $l+1 \to l-1$ and $\Delta\zeta \to -\Delta\zeta$ for $W \geqslant 0$. Non-advection and advection phase are solved in the same way as those for two-dimensional case.

References

[1] T. Yabe, F. Xiao, T. Utsumi, Constrained interpolation profile method for multiphase analysis, J. Comput. Phys. 169 (2001) 556–593.
[2] P.Y. Wang, T. Yabe, T. Aoki, A general hyperbolic solver the CIP method applied to curvilinear coordinate, J. Phys. Soc. Jpn. 62 (1993) 1865–1871.
[3] T. Yabe, H. Mizoe, K. Takizawa, H. Moriki, H. Im, Y. Ogata, Higher-order schemes with CIP method and adaptive Soroban grid towards mesh-free scheme, J. Comput. Phys. 194 (2004) 57–77.
[4] K. Suzuki, N. Fujimatsu, Application of CIP method to viscous supersonic and hypersonic flow analysis around aerospace vehicles, Comput. Fluid Dynam. J. 8 (1999) 113–120.
[5] T. Himeno, T. Watanabe, A. Konnno, Numerical Analysis for Propellant Management in Liquid Rocket Tank, AIAA Paper 2001-3822, 2001.
[6] H. Takewaki, T. Yabe, Cubic-interpolated Pseudo Particle (CIP) method application to nonlinear or multi-dimensional problems, J. Comput. Phys. 70 (1987) 355–372.
[7] D.V. Gaitonde, M.R. Visbal, Pade-type higher-order boundary filters for the Navier–Stokes equations, AIAA J. 38 (11) (2000) 2103–2112.
[8] T. Aoki, Multi-dimensional advection of CIP (cubic-interpolated propagation) scheme, CFD J. 4 (1995) 279–291.
[9] S.T. Zalesak, Fully multidimensional flux-corrected transport algorithm for fluids, J. Comput. Phys. 31 (1979) 335–362.
[10] T. Yabe, F. Xiao, Description of complex and sharp interface during shock wave interaction with liquid drop, J. Phys. Soc. Jpn. 62 (1993) 2537–2540.
[11] M. Ranc~ić, Semi-Lagrangian piecewise biparabolic scheme for two-dimensional horizontal advection of a passive scalar, Mon. Weather Rev. 120 (1991) 1394–1406.
[12] C.A. Doswell II, A kinematic analysis of frontogenesis associated with a nondivergent vortex, J. Atmos. Sci. 41 (1984) 1242–1248.
[13] T. Nakamura, R. Tanaka, T. Yabe, K. Takizawa, Exactly conservative semi-Lagrangian scheme for multi-dimensional hyperbolic equations with directional splitting technique, J. Comput. Phys. 174 (2001) 171–207.